

Global surface solar radiation and photovoltaic power from Coupled Model Intercomparison Project Phase 5 climate models



Ling Zou ^a, Lunche Wang ^{a,*}, Jiarui Li ^a, Yunbo Lu ^a, Wei Gong ^b, Ying Niu ^a

^a Hubei Key Laboratory of Critical Zone Evolution, School of Geography and Information Engineering, China University of Geosciences, Wuhan 430074, China

^b State Key Laboratory of Information Engineering in Surveying, Mapping and Remote Sensing, Wuhan University, Wuhan 430079, China

ARTICLE INFO

Article history:

Received 19 October 2018

Received in revised form

18 March 2019

Accepted 24 March 2019

Available online 25 March 2019

Keywords:

Surface solar radiation

Photovoltaic power

Solar energy

CMIP5

ABSTRACT

In this study, historical surface solar radiation (1850–2005) and future photovoltaic power output (2006–2100) are analyzed to investigate the spatial distribution and long-term variation in global solar energy based on the Coupled Model Intercomparison Project Phase 5 (CMIP5) models and the Global Energy Balance Archive (GEBA) database. The results show that global mean surface solar radiation significantly decreased by $0.014 \text{ W m}^{-2} \text{ year}^{-1}$ in 1850–2005. According to the Model for Interdisciplinary Research on Climate (MIROC5), surface solar radiation significantly decreased by $3.42 \text{ W m}^{-2} \text{ year}^{-1}$ in 1951–1992 and increased by $4.75 \text{ W m}^{-2} \text{ year}^{-1}$ in 1993–2005. Global dimming and brightening were observed before and after the 1990s, respectively. The transition of surface solar radiation from dimming to brightening in Europe and the southeastern United States was detected in the 1980s. Stations in Northeast China, Japan, Southeast Africa, the Middle East, and the west coast of India all showed renewed decreasing trends after the 1990s. The direct and indirect effects of anthropogenic aerosols and cloudiness in different periods and regions were the main causes of the changes. To better understand the utilization of global solar energy, global potential photovoltaic power outputs were estimated in future scenarios with an empirical model. Significant increases in potential photovoltaic power are expected in East Asia, Europe, Central Africa and Central America in 2006–2100. The largest increase is expected in central China, where increases are occurring at $3 \text{ kWh m}^{-2} \text{ year}^{-1}$. Significantly decreasing potential photovoltaic power is observed in North Africa, the Middle East, Central Asia and Australia. The greatest decrease is observed in the Tibetan Plateau area (approximately $-3.0 \text{ kWh m}^{-2} \text{ year}^{-1}$ in 2006–2100). With respect to the global distribution of potential photovoltaic power output, large quantities of photovoltaic power are distributed in the northern and southern parts of Africa, the Middle East, the Tibetan Plateau area, the west coasts of North and South America and most of Australia. The yearly mean sum photovoltaic power in these regions is larger than 2000 kWh m^{-2} . Due to the long-term decreasing photovoltaic power ($0.67 \text{ kWh m}^{-2} \text{ year}^{-1}$) expected worldwide in 2006–2100, effective and rational utilization of solar energy is of great importance.

© 2019 Elsevier Ltd. All rights reserved.

1. Introduction

Renewable energy resources are important due to the depletion of traditional fossil fuel resources and global energy-related environmental changes, especially climate change. Wind and solar power, two of the most promising renewable energy forms, increased by an average of 5.4% with respect to total final energy

consumption during 2005–2015, along with biomass, geothermal power and ocean power (REN, 2018). Solar radiation is drawing increasing attention, as it is a sustainable, inexhaustible and widely available energy source. Solar photovoltaic (PV) systems contribute significantly to the carbon-free power supply, as they convert solar energy into electric power. The PV power generating capacity was 303 GW at the end of 2016, which included 98% of all solar power (electricity) systems, and it grew to 400 GW in 2017 (BPSRWE, 2018; REN, 2017). According to the International Energy Agency (IEA, 2018), power generation from PV is up to 460 TWh, which comprises almost 2% of the world's total electricity generation. An average annual growth of 17% is required from 2017 to 2030 in order to reach the IEA's Sustainable Development Scenario (SDS)

* Corresponding author. Hubei Key Laboratory of Critical Zone Evolution, School of Geography and Information Engineering, China University of Geosciences, Lumo road 388, Hongshan District, Wuhan 430074, China.

E-mail address: wang@cug.edu.cn (L. Wang).

target. Therefore, studies on solar photovoltaics are essential to meet growing sustainable energy demands.

The distribution and intensity of incident solar irradiance are key factors affecting solar photovoltaic power production (Práválie et al., 2019). Credible surface solar radiation data are indispensable for future solar photovoltaic power studies. Surface solar radiation is studied mainly via physical measurements taken at meteorological ground stations, retrieved data from geostationary satellites and the reanalysis of numerical weather prediction models. Global and national solar radiation networks process ground measurements and include NOAA's Surface Radiation budget network (SURFRAD <http://www.srrb.noaa.gov/surfrad/index.html>), the Baseline Surface Radiation Network (BSRN <http://www.bsrn.awi.de/>), the World Radiation Data Centre (WRDC <http://wrdc.mgo.rssi.ru/>) and the Global Energy Balance Archive (GEBA <http://www.geba.ethz.ch/>). Numerous models have been proposed in the last few decades to estimate solar radiation with satellite data. There are some available satellite-based databases, e.g., the Satellite Application Facility on Climate Monitoring (CM SAF <https://www.cmsaf.eu/>), the Solar Data project (SoDa <http://www.soda-pro.com/>), the European Database of Daylight and Solar Radiation (Satel-Light <http://www.satel-light.com>) and so on (Paulescu et al., 2013). Empirical models, physical models and artificial intelligence models are widely used in regional and global solar radiation estimations. Empirical models are meteorological parameter-based models such as temperature-based models, sunshine duration-based models, and relative humidity- and cloud-based models (Besharat et al., 2013; Jahani et al., 2017). Physical models usually take into consideration the atmospheric attenuation processes that occur when solar radiation passes through the atmosphere (Gueymard, 1989; Yang et al., 2006). Artificial intelligence models, such as artificial neural networks (ANN), genetic algorithms (GA), expert systems (ES), and fuzzy logic (FL), are promising for solar radiation prediction (Mellit, 2008; Qazi et al., 2015). Reliable solar radiation data estimated by these models lay the foundation for further studies. A global decrease in surface solar radiation during the 1950s–1980s and an increase in the transition thereafter are described in (Wild, 2009; Wild et al., 2005).

The PV physical or parametric models and statistical or machine learning models are the main forecasting methods (Antonanzas et al., 2016; Voyant et al., 2017). Ding et al. (2011) proposed an artificial neural network approach to accurately and efficiently forecast the power output of a PV system in different weather types. Bonanno et al. (2012) used a radial basis function neural network to estimate accurate PV output with available historical PV data, including solar irradiation and temperature. Rana et al. (2016) used historical PV power data to forecast PV power with an ensemble of neural networks and support vector regression approaches. Schmelas et al. (2015) used three models (a physical model, a multilayer perceptron neural network, and a hybrid model combining both the physical model and the neural network) along with inputs of solar radiation, temperature and relative humidity to forecast PV energy. The historical PV power data are essential for training and validating artificial intelligence models. The physical or parametric models estimate PV power output by establishing the physical relations between surface solar radiation and atmospheric factors. Lorenz et al. (2011) and Yang and Xie (2012) forecasted power output in a PV system by considering measured air temperature and modeled solar radiation; the electrical efficiency of a PV cell or module can be evaluated by examining the physical relations between solar radiation and ambient and reference temperatures. Bizzarri et al. (2013) and Yona et al. (2013) examined the effect of wind velocity on temperature-based PV power forecasting. Crook et al. (2011) examined variations in temperature and solar radiation and investigated how they will affect PV output

worldwide throughout the 21st century. The results show that few increases in PV power are observed in Europe and China, and decreases are observed in the western USA and in Saudi Arabia.

The majority of previous investigations concentrated on short timescale PV power forecasting. A global long-term prediction of PV power in future decades will be indispensable for guiding the reasonable utilization of solar energy. The Coupled Model Intercomparison Project (CMIP) provides global long-term atmospheric data both in historical and future scenarios; these data include surface downward shortwave radiation, ambient temperature, precipitation, total cloud fraction and aerosol optical thickness (Loew et al., 2016; Taylor et al., 2012). The CMIP can be conducive to investigating the historical variation in surface solar radiation and predicting the potential distribution and variation in PV power. In the present study, we first intend to determine the historical variation in global and regional surface solar radiation and its possible relationships with aerosols and cloudiness in past decades. Second, potential photovoltaic power is forecasted with an empirical model, and the global distribution and intensity of potential photovoltaic power are investigated in future scenarios.

2. Data and methodology

In this section, the Coupled Model Intercomparison Project Phase and the Global Energy Balance Archive database were introduced. The empirical models for photovoltaic power prediction and evaluation indices were presented.

2.1. CMIP5

The Coupled Model Intercomparison Project Phase 5 (CMIP5) comprises a set of climate model experiments from 20 climate modeling groups around the world that study the output of coupled atmosphere-ocean general circulation models (AOGCMs). The core simulations in the CMIP5 long-term experiments include an Atmospheric Model Intercomparison Project (AMIP) run, a coupled control run, a historical run (1850–2005) and two future climate change projection scenarios (2006–2100). The historical run is forced by observed atmospheric composition changes (reflecting both anthropogenic and natural sources). Two scenarios are based on future population growth, technological development and societal response, which are identified representative concentration pathways that result in a radiative forcing of 4.5 W m^{-2} (medium emission scenario) and 8.5 W m^{-2} (high emission scenario) at the end of the 21st century compared to the preindustrial state (Taylor, 2009; Taylor et al., 2012). The scenarios are time-dependent, consistent projections of emissions and concentrations of radiatively active gases and particles. According to Bartók et al. (2017), future changes in surface solar radiation are likely best predicted by the RCP8.5 scenario. Therefore, an ensemble run of 36 models of historical experiments and a forcing scenario (RCP8.5) are used to study the worldwide distribution of global solar radiation and PV power; detailed information about the models is listed in Table 1. Sixty atmospheric variables are available in the CMIP5. The present study uses global monthly data including surface downwelling shortwave radiation (RSDS), surface downward clear sky shortwave radiation (RSDSCS), ambient temperature (TAS), total cloud fraction (CLT), and aerosol optical depth at 550 nm (AOD), which are provided by 36 models in the CMIP5.

2.2. Global Energy Balance Archive

The Global Energy Balance Archive (GEBA) database provides worldwide ground-measured global solar radiation data at the Earth's surface (Gilgen and Ohmura, 1999; Wild et al., 2017). It has

Table 1

Information of 36 CMIP5 models.

Model center	Institution	Model name	lon × lat	Historical	RCP8.5
CSIRO-BOM	Commonwealth Scientific and Industrial Research Organization and Bureau of Meteorology	ACCESS1-0	192 × 145	□ ○ △ ✕	□ ○ △ ✕
NCAR	National Center for Atmospheric Research	ACCESS1.3	192 × 145	□ ○ △ ✕	□ ○ △ ✕
CMCC	Centro Euro-Mediterraneo per i Cambiamenti Climatici	CCSM4	288 × 192	□ △ ✕	□ △ ✕
CNRM-CERFACS	Centre National de Recherches Meteorologiques and Centre European de Recherches et Formation Avancees en Calcul Scientifique	CMCC-CESM	96 × 48	□ △ ✕	□ △ ✕
CSIRO-QCCCE	Commonwealth Scientific and Industrial Research Organization in collaboration with the Queensland Climate Change Centre of Excellence	CMCC-CMS	192 × 96	□ △ ✕	□ △ ✕
UNSW	UNSW (University of New South Wales, Sydney, Australia)	CMCC-CM	480 × 240	□ △ ✕	□ △ ✕
CCCma	Canadian Centre for Climate Modelling and Analysis	CNRM-CM5-2	256 × 128	□ ✕	
LASG-IAP	Institute of Atmospheric Physics, Chinese Academy of Sciences	CNRM-CM5	256 × 128	□ △ ✕	□ ✕
NASA-GISS	NASA/GISS Goddard Institute for Space Studies	CSIRO-Mk3-6-0	192 × 96	□ ○ △ ✕	□ ○ △ ✕
NIMR-KMA	National Institute of Meteorological Research	CSIRO-Mk3L-1-2	64 × 56	□ △ ✕	
MOHC	Met Office Hadley Centre	CanCM4	128 × 64	□	
IPSL	Institut Pierre Simon Laplace	CanESM2	128 × 64	□ △ ✕	□ △ ✕
MIROC	Japan Agency for Marine-Earth Science and Technology, Atmosphere and Ocean Research Institute	FGOALS-s2	128 × 108	□ △ ✕	□ △ ✕
MPI-M	Max Planck Institute for Meteorology	GISS-E2-H-CC	144 × 90	□ △ ✕	□ △ ✕
MRI	Meteorological Research Institute	GISS-E2-H	144 × 90	□ ○ △ ✕	□ ○ △ ✕
NCC	Norwegian Climate Centre	GISS-E2-R-CC	144 × 90	□ △ ✕	□ △ ✕
INM	Institute for Numerical Mathematics	GISS-E2-R	144 × 90	□ ○ △ ✕	□ ○ △ ✕
		HadCM3	96 × 73	□ △ ✕	□ △ ✕
		HadGEM2-AO	192 × 145	□ △ ✕	
		HadGEM2-CC	192 × 145	□ ○ △ ✕	□ ○ △ ✕
		HadGEM2-ES	192 × 145	□ ○ △ ✕	□ ○ △ ✕
		IPSL-CM5A-LR	96 × 96	□ △ ✕	□ ○ △ ✕
		IPSL-CM5A-MR	144 × 143	□ ○ △ ✕	□ ○ △ ✕
		IPSL-CM5B-LR	96 × 96	□ △ ✕	□ △ ✕
		MIROC-ESM-Chem	128 × 64	□ ○ △ ✕	□ ○ △ ✕
		MIROC-ESM	128 × 64	□ ○ △ ✕	□ ○ △ ✕
		MIROC4h	640 × 320	□ ○ △ ✕	
		MIROC5	256 × 128	□ ○ △ ✕	□ ○ △ ✕
		MPI-ESM-LR	192 × 96	□ △ ✕	□ △ ✕
		MPI-ESM-MR	192 × 96	□ △ ✕	□ △ ✕
		MPI-ESM-P	192 × 96	□ △ ✕	
		MRI-CGCM3	320 × 160	□ ○ △ ✕	□ ○ △ ✕
		MRI-ESM1	320 × 160	□ ○ △ ✕	□ ○ △ ✕
		NorESM1-ME	144 × 96	□ ○ △ ✕	□ ○ △ ✕
		NorESM1-M	144 × 96	□ ○ △ ✕	□ ○ △ ✕
		inmcm4	180 × 120	□ △ ✕	□ △ ✕

Note: □ denotes the presentation of surface downward shortwave radiation (RSDS) in model, ○ the presentation of aerosol optical thickness at 550 nm (AOD) data in model, △ the presentation of total cloud fraction (CLT) data in model, ✕ the presentation of ambient temperature (TAS) in model.

been widely used for detecting multidecadal variations in global solar radiation and quantifying the global energy balance. Gilgen et al. (2009) analyzed the worldwide decadal variation in surface solar radiation with the GEBA database. Wild et al. (2015a) estimated the global mean energy balance and its representation in the CMIP5 models using GEBA. The GEBA database also plays an important role in assessing surface energy fluxes in climate models, satellite-derived predictions and reanalysis products. For example, Zhang et al. (2016) assessed six representative global reanalysis incident solar radiation products. Li et al. (1995) validated the monthly mean surface insolation from satellite-based ERBE/SRB and GEWEX/SRB with the GEBA database. Müller et al. (2015) validated the surface solar radiation retrieved by CM-SAF SARAH. Ma et al. (2015) evaluated surface incident solar radiation from 48 models in the CMIP5 and reported an overestimation of approximately 11.9 W m^{-2} based on information from the GEBA database. All of the above results indicate the feasibility of the GEBA database in validating modeled or retrieved surface solar radiation. There are a total of 1518 stations from around the world represented by the GEBA database, except for South America. Stations in South America are excluded in this study due to the absence of data. The validation of surface solar radiation in the CMIP5 for South America will not be discussed in this study. Because of the occasional absence of data, 568 stations are reserved for further analysis.

Additionally, 12 stations are selected for detailed analysis. The location and geographic information for the 568 GEBA stations is shown in Fig. 1 and Table A1 in the Appendix.

2.3. Photovoltaic power output forecasting

Solar radiation is the energy source for photovoltaic power (PV) systems, and system operating temperatures strongly affect the electrical efficiency of a PV cell or module. According to Dubey et al. (2013) and Bayrakci et al. (2014), PV power output and electrical efficiency depend linearly on the operating temperature. A lower PV cell/module operating temperature leads to increasing electrical efficiency (increasing PV power output) with a similar incident solar radiation flux. With the high spatial and temporal resolution of surface solar radiation data in the CMIP5, a physical method that is based on temperature and solar radiation flux will be used to forecast photovoltaic power in this study. Skoplaki and Palyvos (2009) and Crook et al. (2011) stated that the photovoltaic power output can be obtained from the photovoltaic cell's electrical efficiency and global solar radiation:

$$P_{pv} = G_{SR} \times \eta_c \quad (1)$$

Where P_{pv} is the photovoltaic power output, G_{SR} is global solar

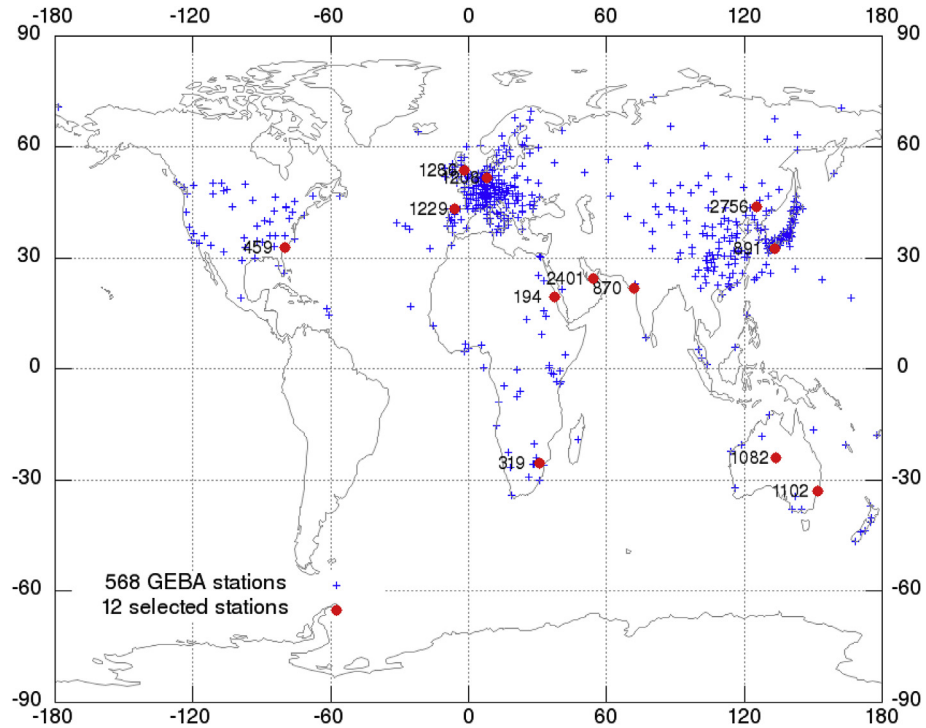


Fig. 1. Distribution of 568 GEBA stations (blue cross) and 12 selected stations (red dot). (For interpretation of the references to color in this figure legend, the reader is referred to the Web version of this article.)

radiation, η_c is the PV cell's electrical efficiency.

$$\eta_c = \eta_{Tref} [1 - \beta_{ref} (T_c - T_{ref}) + \log_{10} G_{SR}] \quad (2)$$

$$T_c = T_a + (T_{NOCT} - T_{a,NOCT}) \times \frac{G_{SR}}{G_{NOCT}} \quad (3)$$

where T_c and T_{ref} are the cell and reference temperatures, respectively (Evans, 1981); η_{Tref} is the cell's electrical efficiency at the reference temperature; β_{ref} and γ are the temperature and solar radiation coefficients determined by the cell's material and structure; T_a is the ambient surface temperature; $NOCT$ is the nominal operating cell temperature, which is defined as the cell or module temperature that is reached when the cells are mounted in the normal way at a solar radiation level of 800 W m^{-2} , a wind speed of 1 m/s and an ambient temperature of 293.16 K (20°C) with $\eta_c = 0$; T_{NOCT} is the model temperature at $NOCT$ conditions, usually 45.5°C ; and $T_{a,NOCT}$ is 20°C (Duffie et al., 1980). As stated in (Skoplaki and Palyvos, 2009), at $T_{ref}=25^\circ\text{C}$, the average η_{Tref} is approximately 0.12, γ is 0.12 and the average $\beta_{ref}=0.0045^\circ\text{C}^{-1}$ for crystalline silicon modules, according to previous studies (Assoa et al., 2007; Nottou et al., 2005).

2.4. Evaluation indices

The root mean square error (RMSE) and the mean absolute error (MAE) are used to evaluate the performances of models in the CMIP5 via data from the ground-measured GEBA database, and the correlation coefficients (R) and R-square are calculated to analyze the relationships between global solar radiation, photovoltaic power and meteorological factors.

$$\text{RMSE} = \sqrt{\frac{1}{n} * \sum_{i=1}^n (x_{m,i} - x_{e,i})^2} \quad (4)$$

$$\text{MAE} = \frac{1}{n} * \sum_{i=1}^n |x_{m,i} - x_{e,i}| \quad (5)$$

$$R = \left(\sum_{i=1}^n (x_{m,i} - \bar{x}_m)(x_{e,i} - \bar{x}_e) \right) \times \sqrt{\sum_{i=1}^n (x_{m,i} - \bar{x}_m)^2} \sqrt{\sum_{i=1}^n (x_{e,i} - \bar{x}_e)^2} \quad (6)$$

where n is the number of data points and $x_{m,i}$ and $x_{e,i}$ are i -th and j -th measured and modeled values, respectively. The units of RMSE and MAE are W m^{-2} .

Trends in surface solar radiation, aerosols, cloud fraction and ambient temperature are estimated with Kendall's tau-based slope estimator (Sen, 1968). The significance of the changes is computed with the Mann-Kendall test (Kendall, 1948; Mann, 1945). The Mann-Kendall test is based on the correlation between the ranks of a time series and their time order, and the test statistic is given by:

$$S = \sum_{k=1}^{n-1} \sum_{i=k+1}^n \text{sgn}(x_j - x_k) \quad (7)$$

$$\text{sgn}(x_j - x_k) = \begin{cases} 1 & \text{if } x_j - x_k > 0 \\ 0 & \text{if } x_j - x_k = 0 \\ -1 & \text{if } x_j - x_k < 0 \end{cases} \quad (8)$$

where x_j and x_k are values for time series of the j -th and k -th values,

and $j > k$.

The variance of S statistic can be calculated by:

$$\text{VAR}(S) = 1/18 \left[n(n-1)(2n+5) - \sum_{p=1}^q t_p(t_p-1)(2t_p+5) \right] \quad (9)$$

where n is the number of observations and q is the number of groups of tied ranks, each with t_p tied observations.

The significance of trends can be tested by:

$$Z = \begin{cases} S - 1/\sqrt{\text{VAR}(S)} & \text{if } S < 0 \\ 0 & \text{if } S = 0 \\ S + 1/\sqrt{\text{VAR}(S)} & \text{if } S > 0 \end{cases} \quad (10)$$

where increasing and decreasing trends are presented with positive and negative Z values, respectively. The trend analysis passed the significant test of 95%, as the absolute values of Z were larger than or equal to 1.96.

3. Results and discussion

The optimal model (MIROC5) was selected for detailed analysis after the comparisons of 36 CMIP5 models. Long-term variations and distributions of the surface solar radiation and potential photovoltaic power were analyzed in 1850–2005 and 2006–2100, respectively. The possible effects of aerosol and cloud on changing surface solar radiation and PV power were evaluated.

3.1. Evaluation of surface solar radiation in 36 CMIP5 climate models

The CMIP5 climate model data provide us with a better understanding of the past, present and future climate. Data evaluation is essential before the data are used. Global measurements of surface solar radiation in the GEBA dataset are used to evaluate the CMIP5 models. Information on GEBA stations can be found in [Table A1 in the Appendix](#). The correlation coefficients, root mean square error (RMSE) and mean absolute error (MAE) of surface solar radiation between the GEBA dataset and the CMIP5 models were calculated. Multistation mean values of R-square, RMSE and MAE for each model are shown in [Fig. 2](#). Lower R-square values are observed in HadGEM2-CC and CMCC-CESM with values of 0.56 and 0.64, respectively. R-square values in other models are larger than 0.7. High RMSE and MAE values are observed in HadGEM2-CC, IPSL-models and CMCC-CESM, in which the RMSE values are on average larger than 30 W m^{-2} and the MAE values are on average larger than 25 W m^{-2} . The MIROC5 models, NorESM models and ACCESS models have better performances with high R-square values (>0.76) and lower RMSEs ($<23 \text{ W m}^{-2}$) and MAEs ($<18 \text{ W m}^{-2}$).

The R-square values, RMSEs and MAEs for 568 stations and 36 models are shown in [Fig. 3](#) to demonstrate how models work at different sites. Sixty percent (364) of the stations have R-square values that are greater than 0.8, and 75% (426) of the stations have R-square values that are greater than 0.7. Approximately 14.7% (84) of stations yield R-square values that are less than 0.5. [Fig. 3](#) shows that persistently high R-square values appear at stations 46–80, 120–140, and 160–370. These stations are mainly distributed in North America, Europe and northern Asia. Unsatisfactory performances are observed at stations 1–40, 480–520 and 535–550, which are mainly distributed in Africa and South Asia. Poor

conditions and inexperienced acquisition of ground measurements in those areas may lead to inferior data measurement quality; high emissions may also influence the accuracy of climate models.

For a more specific analysis, statistical errors between the modeled and measured global solar radiation at 12 globally selected stations are presented in [Fig. 4](#). The locations of the 12 stations are shown in [Fig. 1](#). High statistical errors and the lowest R values are observed in the HadGEM2-CC and IPSL-models at all 12 stations. Except for the green round dot (which represents model HadGEM2-CC), high correlation coefficients and low error values are observed in the other 35 models at stations 459, 1102, 1208, 1229, 1286 and 2401. As shown in [Fig. 1](#), the MIROC5, NorESM- and ACCESS- models are better at simulating surface solar radiation than the other models. With respect to the spatial resolutions of the above models (in [Table 1](#)), the MIROC 5 model has the finest spatial resolution (256×128) and is optimal for further analysis.

3.2. Historical characteristics of surface solar radiation

The global annual mean anomaly surface solar radiation (RSDS) in 36 CMIP5 climate models is shown in [Fig. 5](#). The anomaly values are yearly mean values minus multiyear average values. Long-term anomaly values provide an opportunity to investigate long-term changes. A long-term decrease in global solar radiation is observed from 1850 to 2005. It decreases by $0.014 \text{ W m}^{-2} \text{ year}^{-1}$, which is statistically significant at the 99% confidence interval. There are several sharp decreases in past centuries, including decreases in 1858, 1885, and 1903. In this study, we mainly focus on changes in surface solar radiation after 1950. The global mean surface solar radiation decreases by $0.024 \text{ W m}^{-2} \text{ year}^{-1}$ from 1951 to 2005; it also shows decreasing trends during 1995–1992 and 1993–2005 with values of $-0.028 \text{ W m}^{-2} \text{ year}^{-1}$ and $-0.17 \text{ W m}^{-2} \text{ year}^{-1}$, respectively. The trends of global mean RSDS, TAS, AOD and CLT for each model and in the three time periods are analyzed in [Table 2](#). The spatial distribution of trends in the three time periods in the MIROC 5 models are shown in [Fig. 6a](#) (1850–2005), [6b](#) (1951–1992), and [6c](#) (1993–2005).

In [Table 2](#), significant decreases in RSDS in 1850–2005 and 1951–1992 are observed in 36 models. Increasing AOD is observed in all of the data in the available models. During 1993–2005, most models show increasing trends in surface solar radiation, but 9 models continue to decrease. The trends of AOD are not well coordinated with the RSDS in all models. The CLT shows some clear relationships with changes in the RSDS in this period. A distinctively increasing surface temperature is detected in all of the models. The reduction of global surface solar radiation from 1850 to 1992 is accepted by all models, and inversely increasing trends are detected in most models after 1993. The AOD and CLT are possible driving factors for these increasing trends. As explained in section 3.1, the MIROC5 model is the optimal choice for detailed analysis. The spatial characteristics of the RSDS, TAS, AOD and CLT in the MIROC5 model for different time periods are shown in [Fig. 6 a, b, and c](#).

Decreasing trends in surface solar radiation are detected in most continental areas ([Fig. 6a](#)), especially in East Europe, East and Southeast Asia and Central Africa. Surface solar radiation decreases by more than $0.15 \text{ W m}^{-2} \text{ year}^{-1}$ during 1850–2005. Global increases in TAS, AOD and CLT are observed over 156 years. Significantly increasing AOD and CLT and decreasing TAS are detected in Eastern Europe, East and Southeast Asia and Central Africa. During one of the shorter periods (1951–1992) ([Fig. 6b](#)), decreasing surface solar radiation is a trend seen worldwide. Major reductions are observed in East and Southeast Asia, Central Africa and Central America, where trend values are larger than $0.40 \text{ W m}^{-2} \text{ year}^{-1}$. The reduction of global solar radiation before the 1990s is consistent

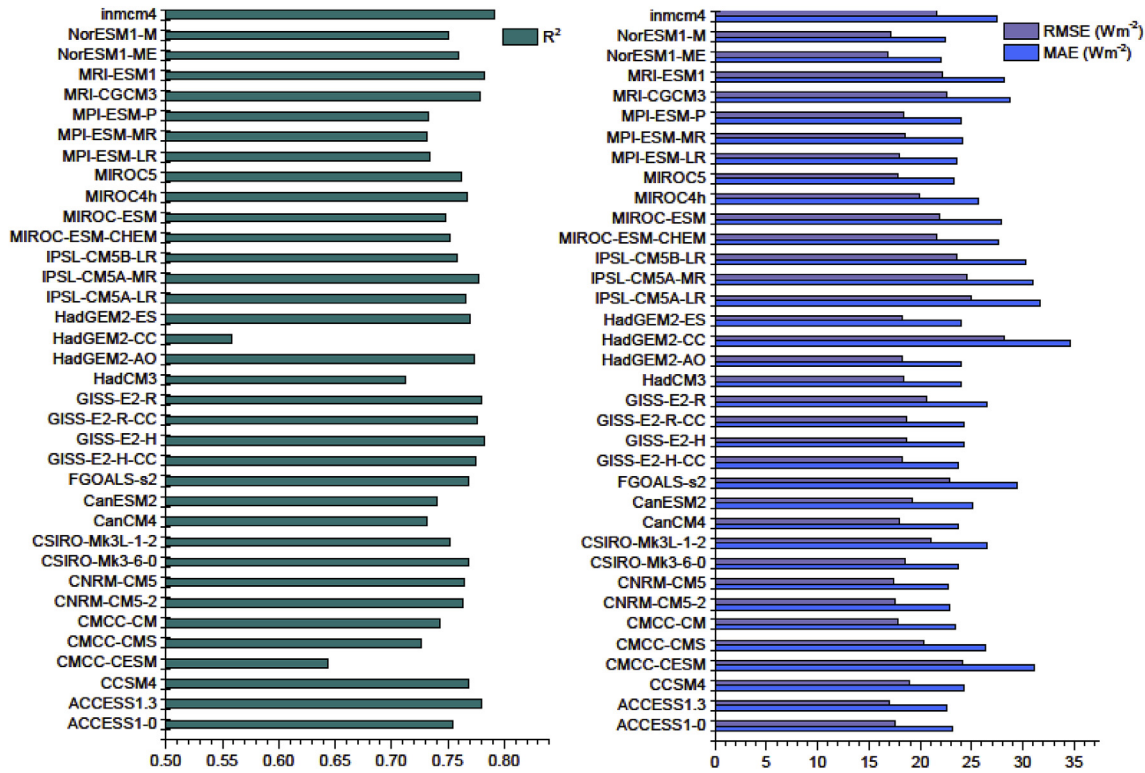


Fig. 2. Comparison of 36 CMIP5 climate models by evaluating the R^2 and statistical errors of modeled and measured surface solar radiation (CMIP5 vs GEBA).

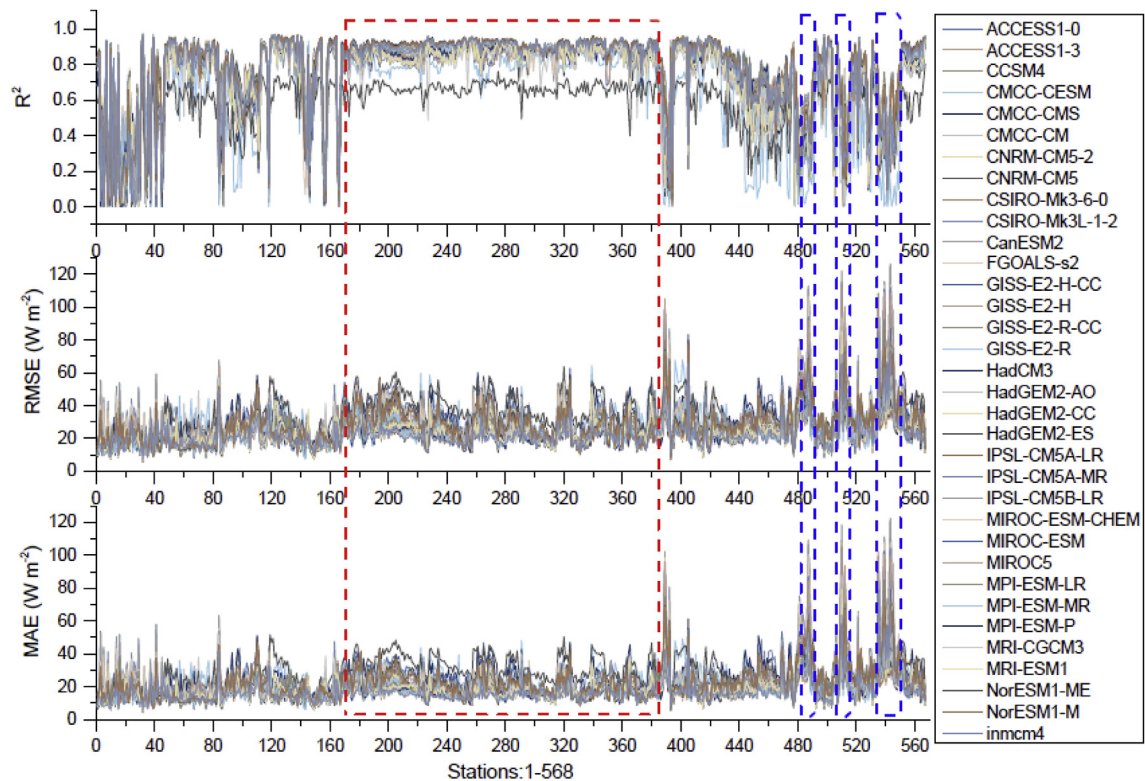


Fig. 3. Statistical errors of surface solar radiation between CMIP5 and GEBA in 568 stations.

with the “dimming” phenomenon showed in previous studies. Stanhill and Cohen (2001) found a global reduction of surface solar radiation from 1958 to 1992 with numerous thermopile

pyranometers that were placed in land-based areas; they concluded that the reduction of surface solar radiation globally averaged $0.51 \text{ W m}^{-2} \text{ year}^{-1}$, and that man-made aerosols and

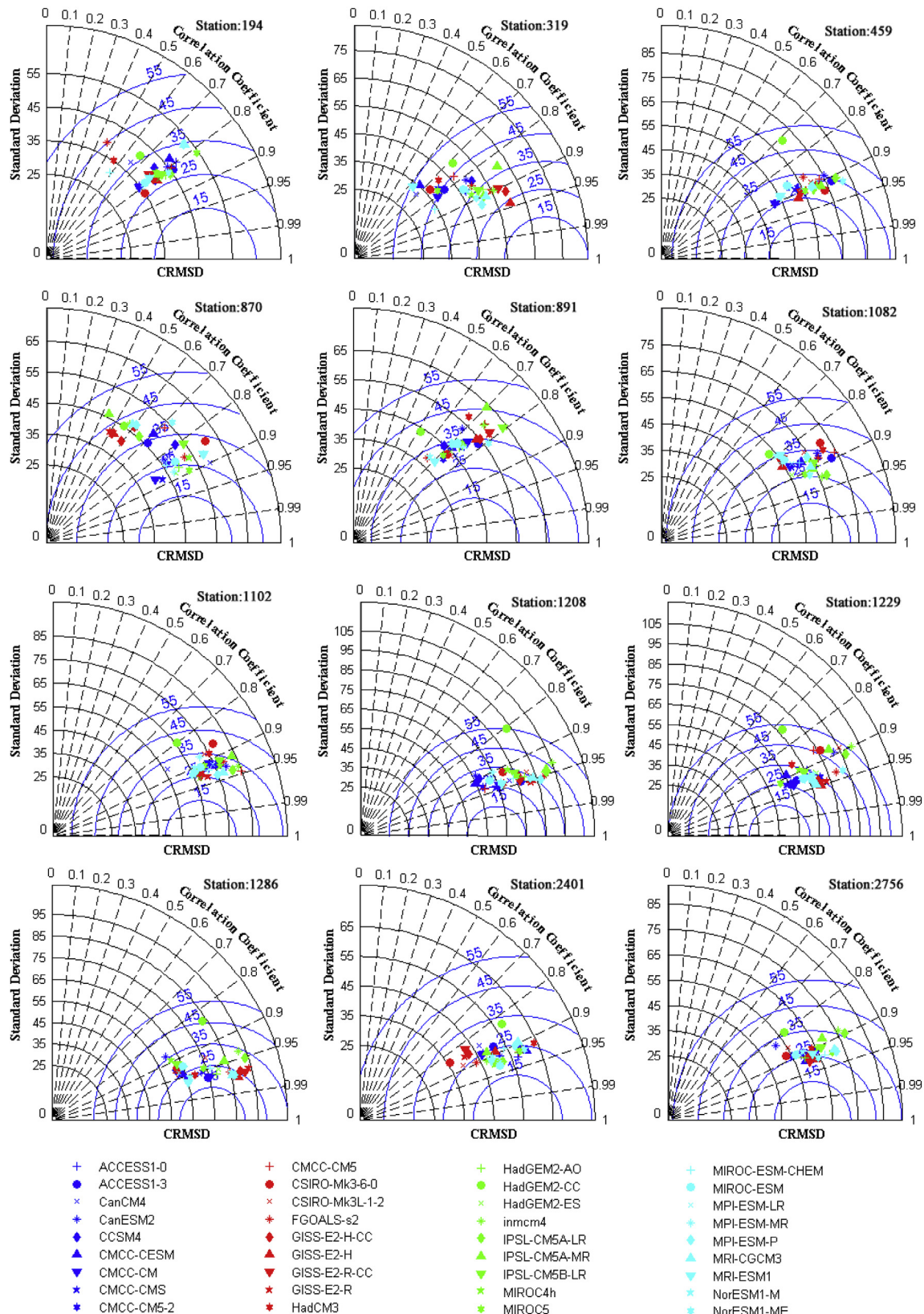


Fig. 4. Statistical evaluation of surface solar radiation between CMIP5 and GEBA in 12 selected stations.

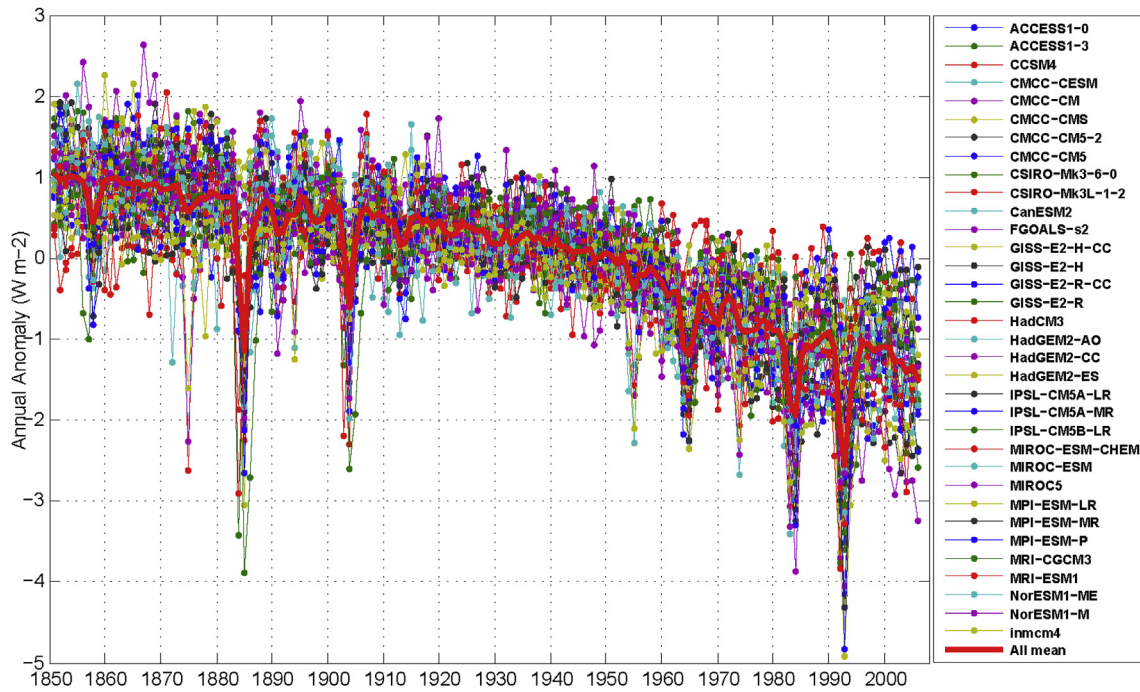


Fig. 5. Global annual mean anomaly surface solar radiation (RSRD) in CMIP5 models during 1850–2005.

Table 2

Trends of surface downward shortwave radiation (RSDS), ambient temperature (TAS), aerosol optical thickness at 550 nm (AOD) and total cloud fraction (CLT) in 36 CMIP5 models for different periods.

Models	1850–2005				1951–1992				1993–2005			
	RSDS	TAS	AOD	CLT	RSDS	TAS	AOD	CLT	RSDS	TAS	AOD	CLT
ACCESS1-0	-1.89	0.37	0.014	0.15	-4.52	1.73	0.032	-0.23	-2.06	4.73	0.006	2.9
ACCESS1-3	-1.73	0.33	0.013	-0.02	-3.48	0.66	0.028	-0.3	-0.44	4.31	0.008	1.67
CCSM4	-1.41	0.79	—	0.47	-3.17	1.74	—	1.39	-1.63	6.92	—	0.53
CMCC-CESM	-1.55	0.15	—	-0.02	-2.29	0.64	—	-0.45	0.07	0.47	—	-0.76
CMCC-CMS	-1.35	0.16	—	-0.22	-1.72	0.78	—	-0.6	1.19	0.86	—	-0.31
CMCC-CM	-1.53	0.38	—	-0.15	-1.89	0.63	—	-0.3	-7.28	2.98	—	0.33
CNRM-CM5-2	-2.47	0.48	—	—	-5.88	1.26	—	—	-1.36	1.35	—	—
CNRM-CM5	-2.43	0.57	—	-0.47	-4.59	0.75	—	-0.96	1.83	7.12	—	-0.22
CSIRO-Mk3-6-0	-2.12	0.48	0.043	-0.19	-4.96	-0.39	0.101	-0.48	2.22	5.11	-0.058	-1.01
CSIRO-Mk3L-1-2	-0.33	0.44	—	-0.16	-1.07	0.71	—	-0.12	2.62	2.5	—	-1.31
CanCM4	-1.46	2.44	—	—	-2.84	0	—	—	1.47	7.19	—	—
CanESM2	-1.4	0.41	—	-0.16	-3.34	1.03	—	-0.51	4.53	6.12	—	-1.83
FGOALS-s2	-2.72	1.15	—	0.48	-5.17	2.3	—	0.89	-4.4	6.92	—	2.85
GISS-E2-H-CC	-2.53	1.01	—	0.39	-5.1	1.41	—	0.92	4.96	5.1	—	0.17
GISS-E2-H	-1.94	0.9	0.041	-0.28	-4.2	1.12	0.121	-0.94	0.23	6.27	-0.046	-0.46
GISS-E2-R-CC	-2.15	0.65	—	0.49	-4.66	0.73	—	1.13	3.94	4.49	—	-1.87
GISS-E2-R	-0.73	0.88	0.042	-0.22	-1.32	1.6	0.124	-0.73	4	3.06	-0.042	2.01
HadCM3	-1.06	0.56	—	-0.18	-2.24	0.57	—	-0.26	1.67	9.65	—	-0.93
HadGEM2-AO	-1.68	0.48	—	-0.02	-3.28	0.52	—	-0.36	2.15	6.71	—	-1.93
HadGEM2-CC	-1.45	0.18	0.017	-0.03	-2.15	0.25	0.015	-0.33	2.52	2.4	0.068	2.82
HadGEM2-ES	-1.63	0.46	0.019	-0.05	-3.12	0.57	0.001	-0.59	-1.99	4.54	0.043	4.54
IPSL-CM5A-LR	-0.73	0.74	—	-0.84	-2.21	1.63	—	-1.49	2.14	7.43	—	-5.29
IPSL-CM5A-MR	-0.57	0.57	0.025	-0.81	-1.56	1.11	0.059	-1.74	8.42	4.43	0.01	-5.35
IPSL-CM5B-LR	-1.16	0.8	—	-0.76	-3.03	1.36	—	-1.36	2.76	3.24	—	-2.18
MIROC-ESM-CHEM	-2.2	0.54	0.017	0.57	-4.38	0.98	0.037	0.93	2.19	3.89	0	6.26
MIROC-ESM	-2.16	0.59	0.018	0.49	-3.25	0.5	0.046	-0.18	4.51	5.15	-0.013	3.55
MIROC4h	-1.04	1.67	0.016	-0.11	-1.53	0.76	0.027	-0.65	4.51	4.16	-0.003	1.47
MIROC5	-1.76	0.56	0.019	0.26	-3.42	0.12	0.034	-0.4	4.75	5.7	0.011	0.4
MPI-ESM-LR	-1.36	0.61	—	-0.26	-2.78	1.59	—	-0.85	1.25	5	—	-0.5
MPI-ESM-MR	-1.36	0.59	—	-0.27	-1.42	1.48	—	-0.51	0.03	5	—	0.63
MPI-ESM-P	-1.2	0.63	—	-0.35	-2.49	1.29	—	-0.53	6.11	6.65	—	-4.63
MRI-CGCM3	-1.06	0.31	0.007	0.16	-4.44	0.67	0.037	0.4	3.55	4.71	-0.15	1.35
MRI-ESM1	-1.38	0.47	0.008	0.23	-3.74	0.9	0.024	0.55	-3.03	3.85	-0.064	3.04
NorESM1-ME	-1.33	0.38	0.025	0.04	-3.33	1.18	0.074	0.12	-0.04	7.33	-0.089	4.52
NorESM1-M	-1.24	0.39	0.024	-0.03	-2.5	1.03	0.073	-0.38	3.31	3.75	-0.069	1.06
inmcm4	-0.76	0.5	—	0.04	-1.59	0.82	—	-0.43	1.36	0.36	—	0.37

Note: bold values means statistically significant at 95 confidence interval, “-” means no data. The units of RSDS, TAS, AOD and CLT are % W m⁻² year⁻¹, % K year⁻¹, % year⁻¹ and % year⁻¹, respectively.

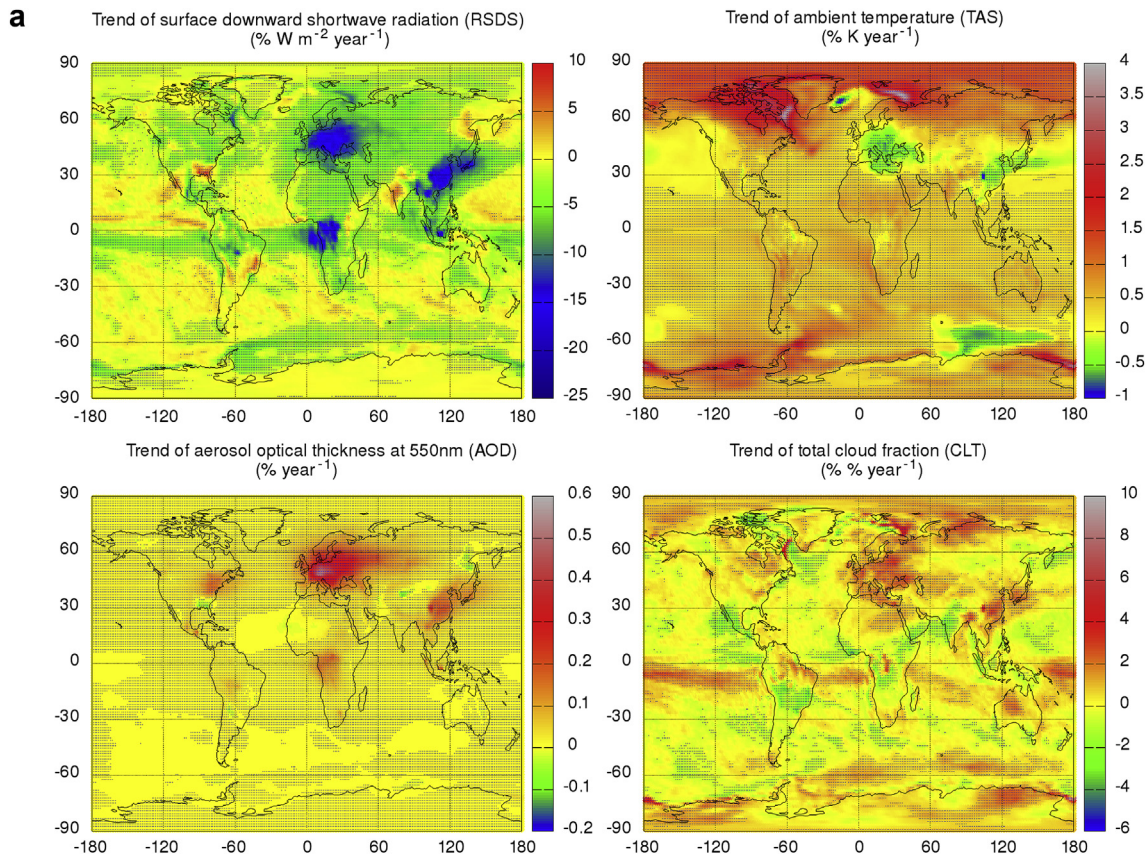


Fig. 6a. Spatial trends of surface downward shortwave radiation (RSDS), ambient temperature (TAS), aerosol optical thickness at 550 nm (AOD) and total cloud fraction (CLT) in MIROC5 during 1850–2005 (light blue dot covered area indicate the statistically significant trends at 95 confidence interval).

other air pollutants were the main possible causes. Liepert (2002) observed a worldwide reduction of surface solar radiation during 1961–1990, equivalent to a 7 W m^{-2} decline in 30 years. In Fig. 6b, slightly decreasing temperatures are observed in Asia, Europe and the Americas. Highly increased AOD and CLT are observed in Europe, East Asia and Central America, which explains the decrease of RSDS in East Asia and Central America. The increasing AOD in Central Africa is a key indicator of decreasing solar radiation.

After 1993 (Fig. 6c), there is a transition in the trend of global surface solar radiation from dimming to brightening. Surface solar radiation increases in most regions, including Europe, North America, North and East Africa, West and Central Asia, central parts of East Asia and most of South America. Significant decreases are found in Southeast Asia, northeastern Asia, and eastern Australia. AOD trends in Europe and Central Africa begin to decrease after 1992. According to Wild (2014) and Wild et al. (2005), the transition from decreasing to increasing solar radiation was observed in Central and Eastern Europe, North America, the former Soviet Union, Japan, China, Australia and India. These changes in atmospheric transmission were possibly caused by direct and indirect aerosol effects. However, the surface solar radiation continues to decrease in Northeast Asia and along its coast, South India and along its coast, and the central and west coasts of Africa. Continuously increasing AOD and CLT may explain the reduction of surface solar radiation. The above results are highly consistent with the study of Gilgen et al. (2009), who demonstrated a shortwave irradiance decrease before 1990 and an increase thereafter. These reverses are observed in Europe, Japan, China, and North America. However, decreases in shortwave irradiance at European coasts and in Central and Northwest China, South India and some parts of

Africa are observed through 2000.

Furthermore, 12 stations are selected according to their spatial distribution. Stations 891 and 2756 are located in East Asia, stations 1102 and 1082 are in Australia, stations 1229, 1208, 1286 are in Europe (Spain, Germany and UK), station 459 is in the southeastern USA, station 319 is in South Africa and stations 194, 2401 and 870 are in the Arabian Peninsula and India (in Fig. 1). The trends of RSDS, AOD, and CLT in the three periods, which are divided by the long-term variations in the global mean RSDS, are shown in Table 3. The annual mean anomalies of RSDS, AOD and CLT from 1850 to 2005 are presented in Fig. 7a, b, and c.

A long-term decrease in the RSDS was observed at Station 2756 (Northeast China) from 1951 to 2005 with values of $-0.22 \text{ W m}^{-2} \text{year}^{-1}$ and $-0.56 \text{ W m}^{-2} \text{year}^{-1}$ for 1951–1992 and 1993–2005, respectively, according to Table 3. In Fig. 7a, decreasing RSDS is observed in the 1960s to 2000. A persistently significant increase in AOD was detected after the 1950s, which may be attributed to long-term dimming at these stations. The CLT trends are negative in Table 3, but we can find a slight increasing trend after the 1960s in Fig. 7a. Similar trends of solar radiation at a station in Harbin (a city in Northeast China) have been investigated (Wild et al., 2009). These investigations supposed that the rebound of anthropogenic sulfur emissions accompanied by increased cloudiness would be the main reason for the dimming after 2000. Xia (2010) reported renewed dimming after 2000 in North China and reasoned that the decreased atmospheric transparencies after 1991 caused the renewed dimming. The same trends in surface solar radiation, cloud fraction, and aerosol optical depth observed at other stations in northeastern China were also analyzed (Tang et al., 2017; Wang and Wild, 2016). Similar trends were observed at Station 891

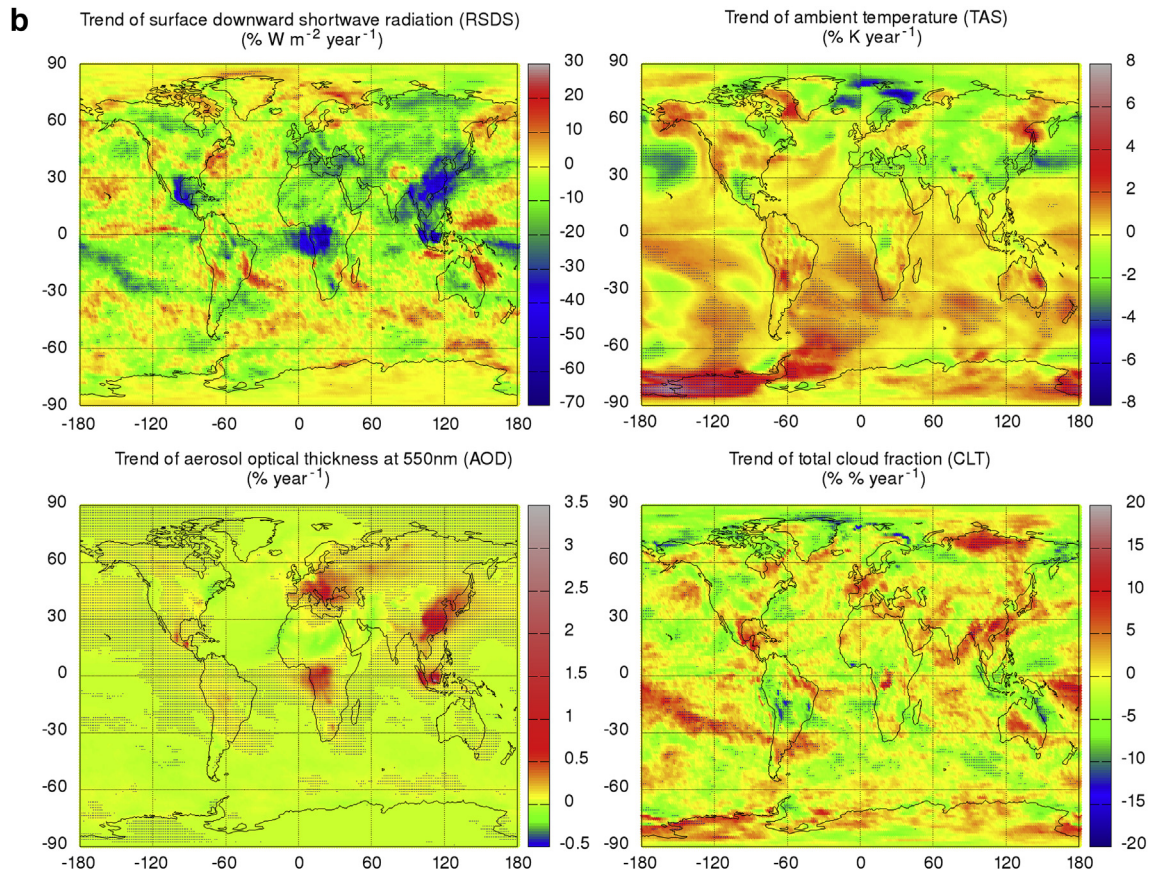


Fig. 6b. Spatial trends during 1951–1992.

(Japan); RSDS decreased from the 1950s to the 1980s and slightly increased from the end of the 1980s to the 2000s. Increasing AOD and CLT were detected after 1950. Ohmura (2009) and Norris and Wild (2009) described the variations in Japan and found an increasing surface solar radiation between the 1990s and 2000s after dimming in 1960–1980. The effects of changes in cloud cover and the direct and indirect effects of aerosols both played important roles in changing global solar radiation in Japan. Station 1102 (east coast of Australia) showed an increasing trend of RSDS in 1970–1980 after the dimming that occurred before the 1970s; this increase was followed by a reduction after 1980. Sharp reductions of AOD and CLT were detected around the year 1980 at this station; a similar trend was observed at station 1082. There is no clear reason for brightening in these years. According to Cohen et al. (2004), a continuous downward trend for evaporation was observed in the 1990s to 2002, which may explain the dimming observed in Australia. Although Wild et al. (2005) suggested an increase in solar radiation after 1993, the researchers averaged its variation over the whole of Australia. In Fig. 6c, we can clearly find decreasing trends in the eastern coastal areas of Australia. The significant increase in CLT may be the main reason for this decrease. Station 319 is located in South Africa, where the RSDS shows a significant continuing downward trend; here, the AOD and CLT increased from 1950 to 2005 (Fig. 7a). The same variations were observed by Ohmura (2009) and Wild et al. (2005). The significant decreases in global solar radiation in South Africa might be caused by volcanic dusts produced after major volcanic eruptions, which was explained by Cohen et al. (2004).

At three stations in Europe (stations 1229, 1208, and 1286), long-term changes of RSDS were observed in the 1970s for stations

1208 and 1286 and in 1980 for station 1229. Surface solar radiation decreased from 1950 on and then increased after the 1970s or 1980s. The value increased by 0.24 and $0.08 \text{ W m}^{-2} \text{ year}^{-1}$ from 1981 to 2005 at stations 1208 and 1286, respectively. Trends of AOD and CLT are in contrast with RSDS in this period; they significantly increased before the 1970s/1980s but decreased thereafter (Fig. 7b). Alpert et al. (2005) found a decline in solar radiation in Europe with a slope of $-0.27 \text{ W m}^{-2} \text{ year}^{-1}$ from 1964 to 1989. Sanchez-Lorenzo et al. (2015) suggested a mean increase of surface solar radiation of approximately $0.2 \text{ W m}^{-2} \text{ year}^{-1}$ after the 1980s over Europe; they mentioned that a decrease in the cloud radiative effects rather than aerosol variations resulted in the increasing solar radiation in Europe. However, Nabat et al. (2013) determined that the decrease in sulfate AOD ranged from -0.05 to -0.19 over Europe from 1979 to 2009, and the maximum AOD (0.32) was observed in the 1980s. The above studies proved that changes in surface solar radiation in Europe and aerosol effects played important roles. There was a long-term increase in surface solar radiation before the 1970s at Station 459 (eastern USA), but a sharp drop was observed in the 1970s–1980s. Liepert and Tegen (2002) investigated the 7 W m^{-2} decrease in solar radiation from the 1970s to the 1980s in the eastern USA. As the aerosol forcing is approximately $1\text{--}2 \text{ W m}^{-2}$, the sharp reduction in this period remains unclear. Long et al. (2009) found widespread brightening in the continental United States from 1995 to 2007 and explained that changes in cloudiness and aerosol effects both led to changes in surface solar radiation.

At station 870 (India), an increase in RSDS was detected from the 1920s to the 1970s, and a decrease was observed after the 1980s. In Fig. 7c, a continuing increase in AOD was investigated after the 1950s, but a slight reduction in CLT was detected from the 1980s

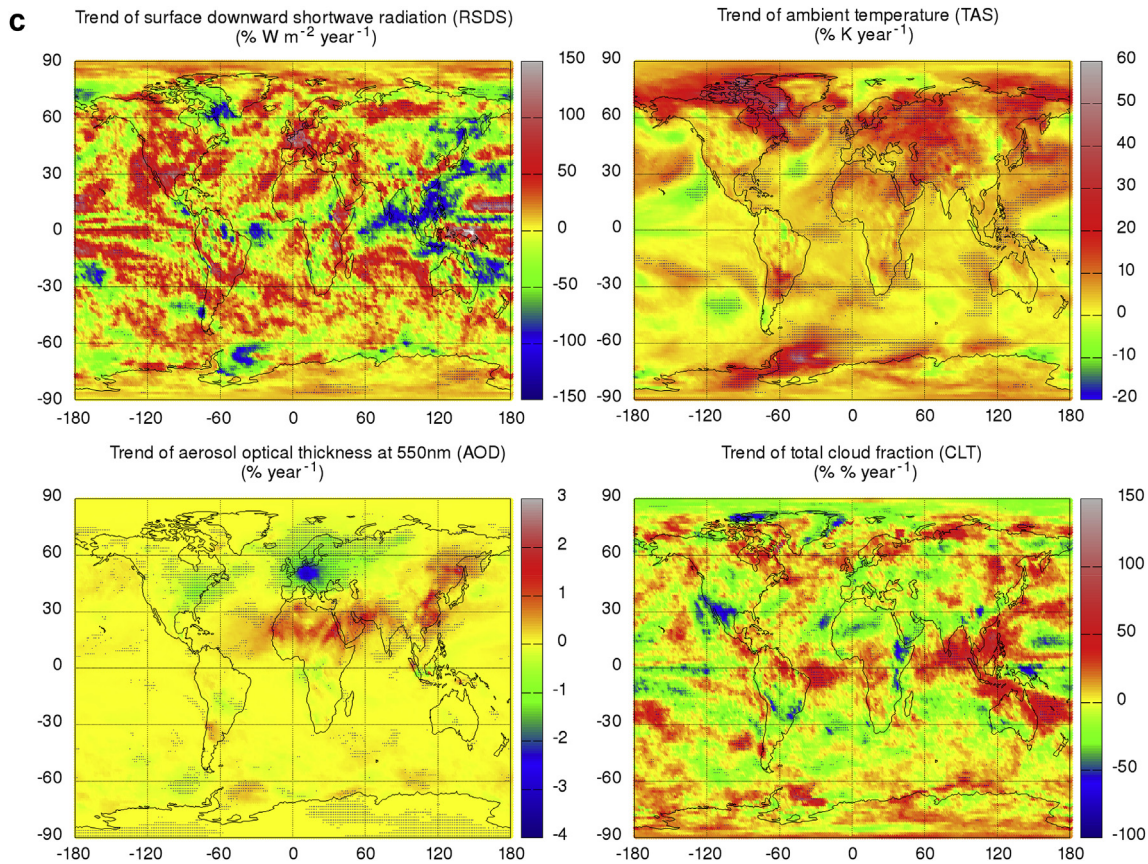


Fig. 6c. Spatial trends during 1993–2005.

Table 3

Selected 12 stations' trends of surface downward shortwave radiation (RSDS), ambient temperature (TAS), aerosol optical thickness at 550 nm (AOD) and total cloud fraction (CLT) in MIROC5 for different periods.

Stations	1850–2005				1951–1992				1993–2005			
	RSDS	TAS	AOD	CLT	RSDS	TAS	AOD	CLT	RSDS	TAS	AOD	CLT
194	-3.17	0.60	0.02	0.47	-12.08	-0.15	-0.02	0.10	-51.25	11.56	2.08	2.10
319	-9.96	0.39	0.10	0.36	-34.98	0.44	0.33	0.97	17.61	6.36	0.17	-7.91
459	6.44	0.45	-0.07	-0.37	-2.75	0.03	0.04	-2.22	17.53	4.38	-0.23	-1.06
870	1.93	0.43	0.02	-1.46	-2.84	0.16	0.05	-2.70	-20.87	3.13	0.26	5.09
891	-9.25	0.01	0.08	1.04	-19.37	-0.58	0.23	-0.13	-44.21	6.43	0.28	19.52
1082	-3.61	0.42	0.00	1.99	-13.34	0.66	0.03	7.43	-27.51	-0.51	-0.05	0.61
1102	-2.75	0.54	0.01	0.68	-12.19	0.30	0.04	6.04	-15.02	2.81	0.00	-9.78
1208	-12.37	-0.24	0.39	1.54	-14.60	0.13	0.16	3.95	104.79	11.65	-2.75	-26.00
1229	-7.67	0.12	0.08	0.40	-18.67	-0.98	0.28	2.57	13.19	3.96	-0.28	-2.26
1286	-5.49	0.22	0.16	1.10	-8.42	-0.19	0.03	4.14	4.75	10.29	-1.20	18.80
2401	-3.27	0.45	0.04	0.22	-12.77	0.08	0.05	3.06	27.16	11.80	0.95	-18.50
2756	-7.45	-0.11	0.10	0.75	-22.04	-1.36	0.34	-0.31	-56.35	-0.92	0.64	-8.33

Note: bold values means statistically significant at 95 confidence interval. The units of RSDS, TAS, AOD and CLT are $\% \text{W m}^{-2} \text{year}^{-1}$, $\% \text{K year}^{-1}$, $\% \text{year}^{-1}$ and $\% \% \text{year}^{-1}$, respectively.

until the end of the 1990s. The increasing anthropogenic aerosols may be a key explanation for the dimming that occurred after the 1980s on the west coast of India. Padma Kumari et al. (2007) and Padmakumari et al. (2017) proved that for solar dimming in the 1980s–2000s over India, AOD and clouds together contributed to the trends. Reductions in solar radiation were observed at stations 194 and 2401 after the 1950s. There were some slight increases in AOD after the 1990s at these two stations, but the long-term trends were not as significant as at other stations. Cloudiness may contribute to the dimming observed in the 1960s to the 1990s, but increasing aerosols are the main driver after the 1990s.

Changes in surface solar radiation show distinct characteristics in different regions. We divided the studied time periods into 1951–1992 and 1993–2005 according to the global mean surface solar radiation shown in Table 3 for the 12 stations. However, changes at the 12 stations shown in Fig. 7a,b,c did not follow the transition. New dimming trends are observed at stations in Northeast China, Japan, the south coast of Africa and the east coast of Australia after the 1990s. A rebound of surface solar radiation in Europe was detected in the 1980s, which is earlier than the average global trends (1990s). The RSDS in the eastern United States shows a sharp drop between the 1970s and 1980s. The direct and indirect

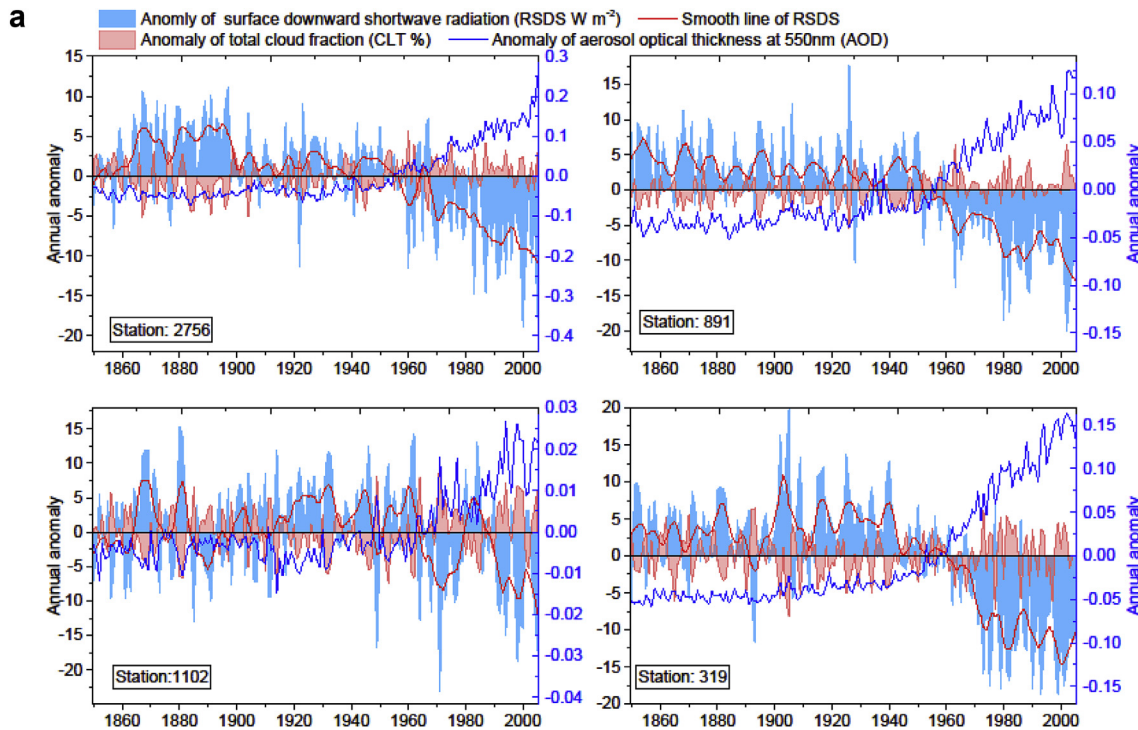


Fig. 7a. Anomaly variations of surface downward shortwave radiation (RSDS), aerosol optical thickness at 550 nm (AOD) and total cloud fraction (CLT) at stations 2756, 891, 1102 and 319.

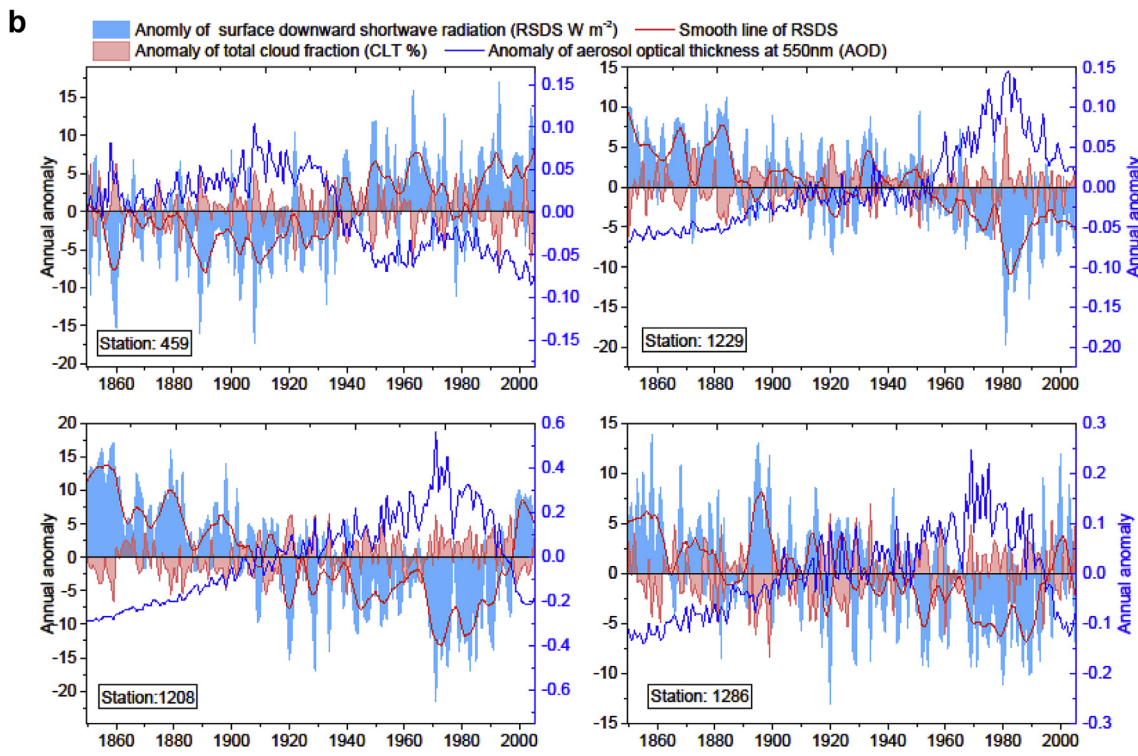


Fig. 7b. At stations 459, 1229, 1208 and 1286.

effects of aerosol emissions and cloudiness have been proven to contribute to variations in surface solar radiation. We would like to suggest that local and regional studies, rather than studies conducted on a global or continental scale, are better for detecting long-term changes in solar radiation and determining its distinctive drivers.

3.3. Changes on potential photovoltaic power

Global potential photovoltaic power (PV) is calculated with equations (1)–(3) in section 2.3 with the surface solar radiation and ambient temperature data obtained from future scenarios. As mentioned in section 2.1, the future change of surface solar

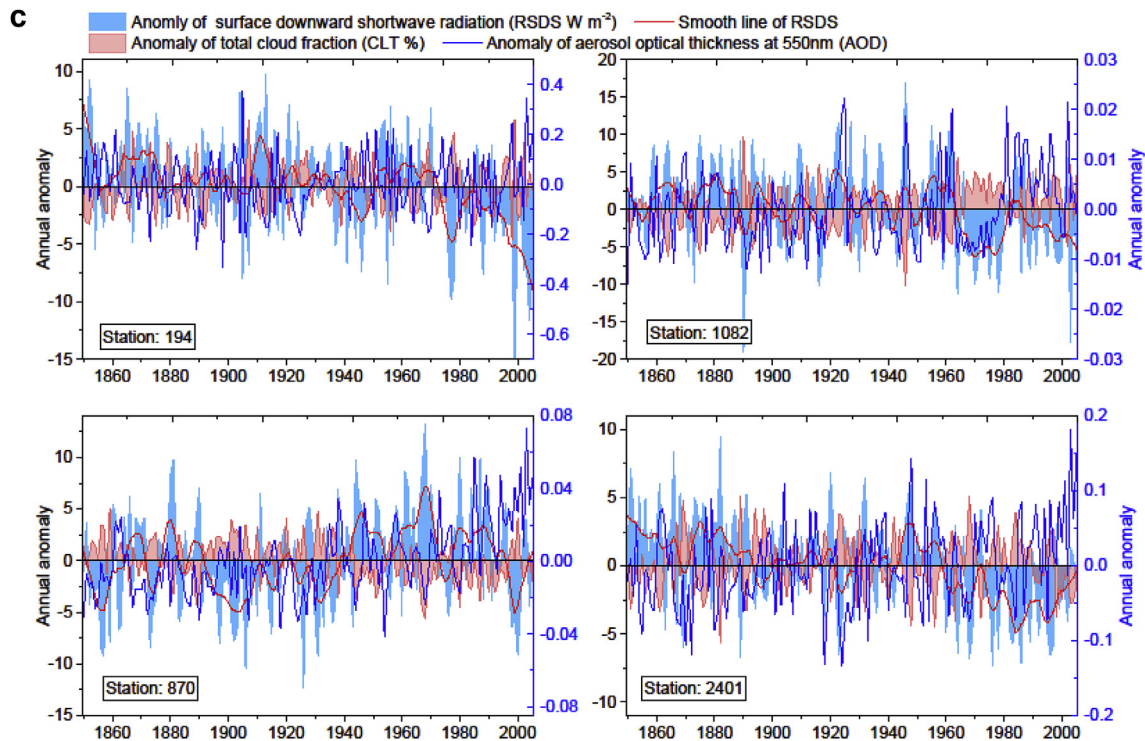


Fig. 7c. At stations 194, 1082, 870 and 2401.

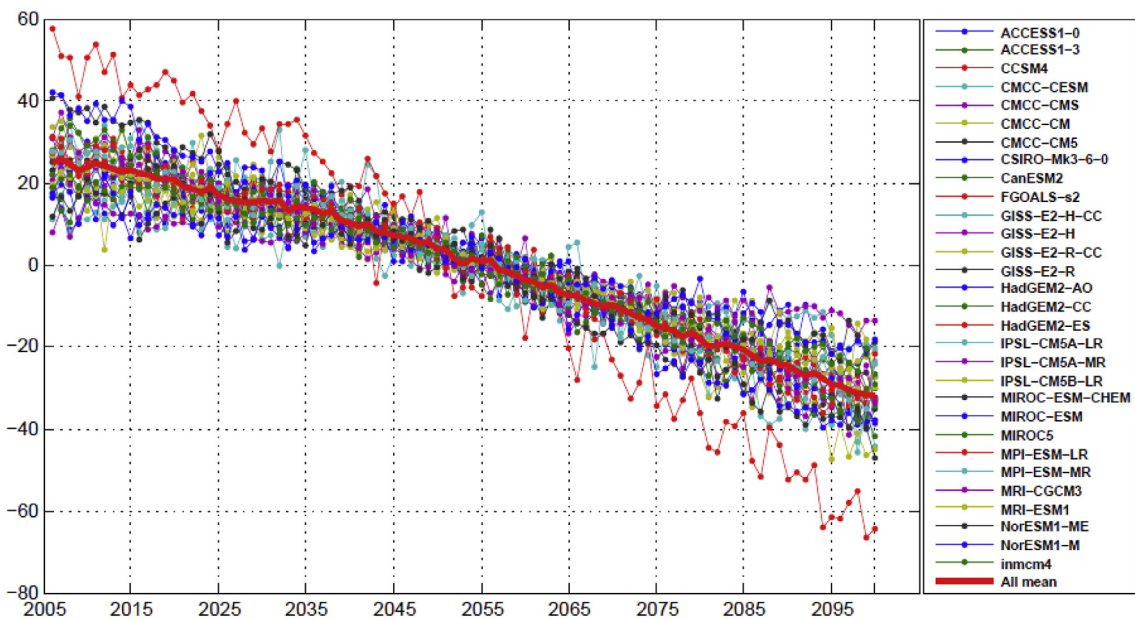


Fig. 8. Global annual mean anomaly potential photovoltaic power (PV) in 36 CMIP5 models in RCP8.5 scenario (2006–2100).

radiation is likely best represented in the scenario of RCP8.5, and the calculation and analysis of photovoltaic power use data only from the RCP8.5 scenario of the CMIP5 models. The global annual mean anomaly potential photovoltaic power in 2006–2100 is shown in Fig. 8. An overall decreasing trend is detected in all models, and the mean PV power of the multi-models decreases by $0.67 \text{ kWh m}^{-2} \text{ year}^{-1}$ during this period. Spatially, trends of PV power, AOD and CLT are shown in Fig. 9. Significant increasing trends of PV power are found in East Asia, Europe, Central Africa,

the northern part of South America, Central America, and especially in central and eastern China, where the PV power increases by approximately $2 \text{ kWh m}^{-2} \text{ year}^{-1}$. Meanwhile, North Africa, Central Asia, Australia, and especially the Tibetan Plateau see decreasing trends of PV power in 2006–2100. Compared with PV power, we find that decreasing trends of AOD, which accompany decreasing CLT, are observed in East Asia, Eastern Europe and the northern part of South America. Increasing AOD in North Africa (Sahara region) may explain the decreasing PV power, while the increasing CLT may

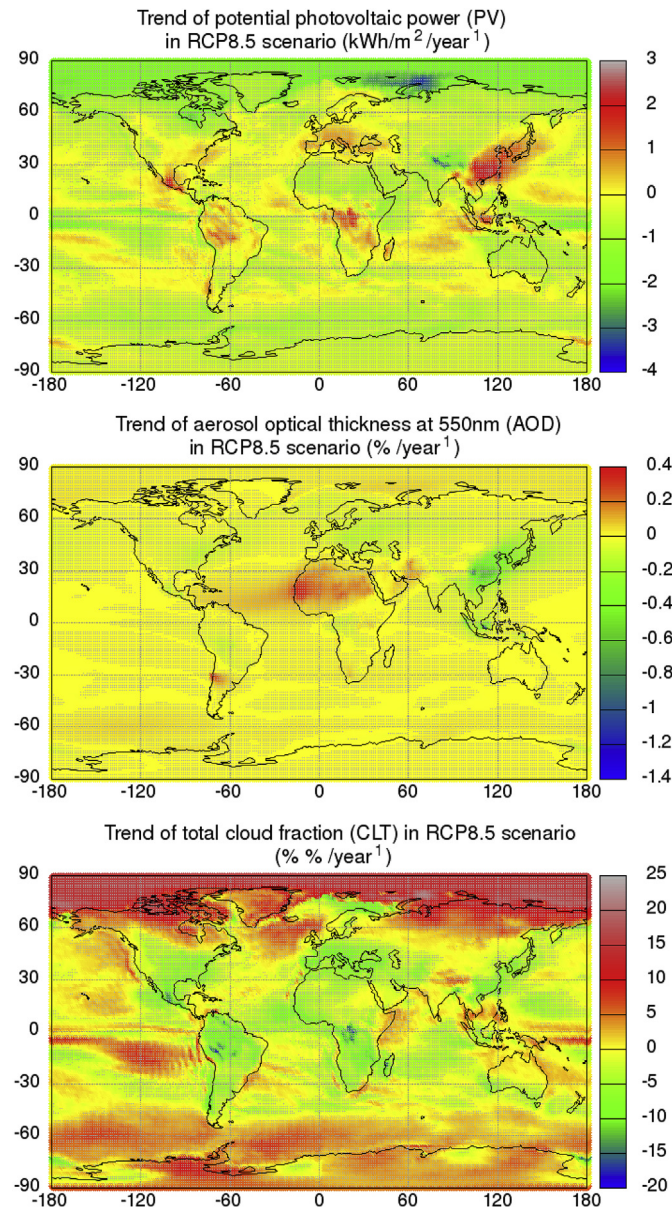


Fig. 9. Trends of potential photovoltaic power (PV), aerosol optical thickness at 550 nm (AOD) and total cloud fraction (CLT) in MIROC5 in RCP8.5 scenario (2006–2100).

contribute to the decrease of PV power in the Tibetan Plateau area. Crook et al. (2011) predicted that PV output will increase in Europe and China and decrease in the western USA and Saudi Arabia from 2010 to 2080 according to climate models HadGEM1 and HadCM3, which are in line with our results in model MIROC5. Wild et al. (2015b) also found significant decreases in PV output in large parts of the world, but positive trends are detected in Europe, the southeastern USA and Southeast China under the RCP8.5 scenario.

Trends in potential PV power, AOD and CLT at 12 stations are shown in Table 4. A significant increase in PV power is found at stations 2576 ($0.53 \text{ kWh m}^{-2} \text{ year}^{-1}$), 891 ($0.72 \text{ kWh m}^{-2} \text{ year}^{-1}$), 1229 ($0.79 \text{ kWh m}^{-2} \text{ year}^{-1}$), 1208 ($0.45 \text{ kWh m}^{-2} \text{ year}^{-1}$), and 391 ($0.39 \text{ kWh m}^{-2} \text{ year}^{-1}$). Slightly increasing trends are observed at stations 459 ($0.15 \text{ kWh m}^{-2} \text{ year}^{-1}$) and 1286 ($0.16 \text{ kWh m}^{-2} \text{ year}^{-1}$). The long-term AOD and CLT in those stations both show significant decreasing trends. Decreasing PV power is detected at stations 194 ($-0.90 \text{ kWh m}^{-2} \text{ year}^{-1}$), 870 ($-0.76 \text{ kWh m}^{-2} \text{ year}^{-1}$), 1082 ($-0.52 \text{ kWh m}^{-2} \text{ year}^{-1}$), 1102 ($-0.44 \text{ kWh m}^{-2} \text{ year}^{-1}$) and 2401 ($-0.71 \text{ kWh m}^{-2} \text{ year}^{-1}$), which are located in Australia, the west coast of India and Saudi Arabia. Increasing AOD detected at stations 194 ($0.18\% \text{ year}^{-1}$) and 2401 ($0.07\% \text{ year}^{-1}$) may contribute to the decreasing PV power observed at those stations. In addition, the significant increase in CLT at station 870 ($1.56\% \text{ year}^{-1}$) may explain its decreasing PV power. By analyzing the correlation coefficients between PV and AOD as well as PV and CLT, we find that except for stations 194 and 2401, the PV power at other stations is negatively correlated with CLT. Significant negative correlation coefficients between PV power and AOD are observed at stations 194 (-0.55), 319 (-0.63), 459 (-0.40), 891 (-0.64), 1208 (-0.55), 1229 (-0.61), 1286 (-0.35) and 2756 (-0.59). Changes in AOD at the abovementioned stations may contribute to variations in surface solar radiation. The increasing PV power at stations 2756, 891 (East Asia), 319 (South Africa), 459 (eastern USA) and 1208, 1229, and 1286 (Europe) may be attributed to both decreasing AOD and decreasing CLT. Significant increases in AOD cause long-term decreasing PV power at stations 194 and 2401, and significant increases in CLT affect the PV power changes at station 870. Gaetani et al. (2014) reported reductions in aerosol emissions from 2000 to 2030 in Europe and North Africa. They found a statistically significant reduction of photovoltaic energy, which is contrary to our results. Therefore, additional information on the trends of PV power is shown in Figure A1a, b, and c in the Appendix. We believe that different study periods produce different results. While the long-term trends of potential PV power are analyzed above, the two-year spatial distribution of global PV power is presented in Fig. 10. An analysis of the long-term trends of PV power, shown in Fig. 9, shows that a slightly bleached red color (representing high

Table 4

Trends of potential photovoltaic power (PV), aerosol optical thickness at 550 nm (AOD) and total cloud fraction (CLT) and correlation coefficients between PV-AOD and PV-CLT in MIROC5 from 2006 to 2100.

Stations	Trends of PV	Trends of AOD	Trends of CLT	r of PV-AOD	r of PV-CLT
194	-0.90	0.18	0.23	-0.55	-0.35
319	0.39	-0.10	-4.36	-0.63	-0.91
459	0.15	-0.03	-5.88	-0.40	-0.86
870	-0.76	-0.01	1.56	0.05	-0.72
891	0.72	-0.15	-2.82	-0.64	-0.89
1082	-0.52	0.00	-0.45	0.54	-0.88
1102	-0.44	-0.01	-2.07	-0.18	-0.85
1208	0.45	-0.05	-6.18	-0.55	-0.88
1229	0.79	-0.03	-8.66	-0.61	-0.92
1286	0.16	-0.03	-3.14	-0.35	-0.92
2401	-0.71	0.07	-2.20	-0.14	-0.41
2756	0.53	-0.29	-2.51	-0.59	-0.83

Note: bold values means statistically significant at 95 confidence interval. The units of PV, AOD and CLT are $\text{kWh m}^{-2} \text{ year}^{-1}$, $\%\text{ year}^{-1}$ and $\%/\text{year}^{-1}$, respectively.

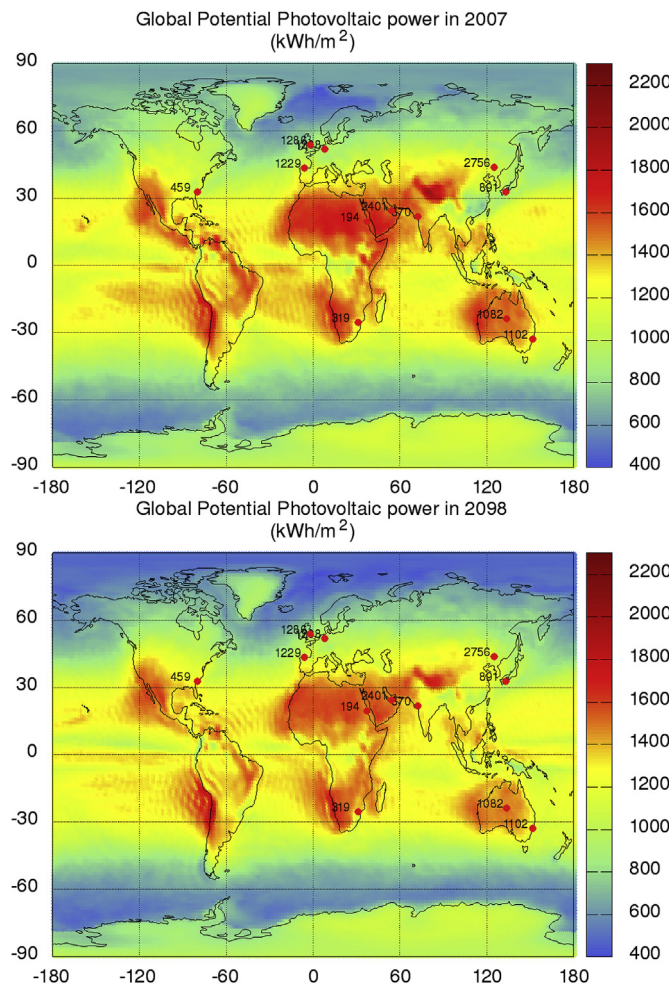


Fig. 10. Global potential photovoltaic power distribution in 2007 and 2098 in RCP8.5 scenario.

PV power regions) is observed for North Africa, South Africa, Central Asia, the Tibetan Plateau, Australia and the west coast of the USA from 2007 to 2098. The photovoltaic power in East Asia, Europe and Central Africa is slightly increased. Jerez et al. (2015) showed the increases in power installed for PV from 2012 to 2020. Comparing global PV power in Fig. 10 with PV output provided at <https://globalsolaratlas.info/>, we find that high potential photovoltaic power is mainly distributed in North and South Africa, the Middle East, West India, the Tibetan Plateau, Australia, and the west coasts of North and South America.

According to Ritchie and Roser (2019), the installed solar photovoltaic capacity was mainly concentrated in Europe, Eurasia, North America, the Asian Pacific, South Africa and Australia in 2016. China, the United States and India are the three countries with the greatest solar PV consumption. The USA, Germany, China and Japan, respectively, shared 12.8%, 10.6%, 32.8% and 12.3% of all cumulative installed photovoltaic power in 2017. The growth rates of installed PV power were 1271.3%, 325.0%, 102.2%, 82.6% and 78.0% in Brazil, Turkey, India, Algeria and Pakistan, respectively, in 2017 (BPSRWE, 2018). The above regions and countries coincide with the high potential photovoltaic power distribution regions shown in Fig. 10, which informs the rational and efficient utilization of surface solar radiation on earth. In addition, we recommend better utilization of solar energy in North Africa, the west coast of South America and Australia because the highest potential PV power is detected in

these locations.

4. Conclusion

Investigating the long-term variation and spatial distribution of surface solar radiation and potential photovoltaic power output is of great importance to the optimal exploitation of solar energy. Therefore, historical and future variations in and distributions of global surface solar radiation and photovoltaic power output are analyzed in this work using the CMIP5 climate models.

The results show that the mean global surface solar radiation of the multi-models significantly decreased by $0.014 \text{ W m}^{-2} \text{ year}^{-1}$ in 1850–2005. After evaluating the surface solar radiation data in the CMIP5 models with respect to GEBA measurements of global solar radiation, we chose the MIROC5 model for further analysis. The global surface solar radiation experienced a significant decrease in 1951–1992 ($-3.42 \text{ W m}^{-2} \text{ year}^{-1}$) and an increase ($4.75 \text{ W m}^{-2} \text{ year}^{-1}$) in 1993–2005. Global dimming and global brightening in these two periods are consistent with the results of other studies (Wild, 2012, 2014). Major reductions in surface solar radiation in 1951–1992 are observed in East and Southwest Asia, Central Africa and Central America. Brightening in 1993–2005 was detected in Europe, North Africa and along the west coast of the USA. In a regional detailed analysis, stations in Europe and the southeastern USA experienced the transition from dimming to brightening; however, at these stations, this transition appeared in the 1980s instead of the 1990s. Stations in Northeast China, Japan and Southeast Africa show continuously decreasing trends after 1960. The maturing energy industry and the use of new forms of energy in Europe and the USA after the 1980s may be the reasons for the recovery of surface solar radiation as sulfate aerosols decreased (Nabat et al., 2013). Increasing aerosols due to industry emissions in Northeast China may cause a continuous decrease in RSRS, and an increase in clouds on the east coast of Australia may contribute to a dimming after the 1990s. The decadal variation in surface solar radiation is largely attributed to changes in aerosols and clouds.

Future global potential photovoltaic power is estimated with empirical models based on the RCP8.5 model scenario. Significantly increasing potential photovoltaic power is detected in East Asia, Europe, Central Africa and Central America. The largest increase is observed in central China, where increases are occurring at a rate of $3 \text{ kWh m}^{-2} \text{ year}^{-1}$ in 2006–2100. Decreasing aerosols seem to be the main reason for the increasing PV in East Asia, and the significant reductions may be the reason for the increasing PV in Europe, Central Africa and America as well. Significantly decreasing PV output is observed in North Africa, the Middle East, Central Asia and Australia. Increasing aerosols and clouds can explain the decreases in North Africa and the Tibetan Plateau. High installed solar PV capacity in the United States, Germany, China and Japan and high growth rates of installed solar PV capacity in Brazil, Turkey, India, Algeria and Pakistan (BPSRWE, 2018; Ritchie and Roser, 2019), which are economically well-developed and rapidly developing regions, are consistent with the increasing PV trends described in this work. These trends suggest that the utilization of renewable energies is highly related to economic levels. In addition to the abovementioned areas, we recommend better utilization of solar energy in North Africa, the west coast of South America and Australia due to their high potential PV power output.

The spatial-temporal variations in surface solar radiation and photovoltaic power production are analyzed in detail in this study based on the CMIP5 climate models and the GEBA database. The results reported in this work help us better understand the spatial and temporal characteristics of surface solar radiation and predict changes in and distributions of potential photovoltaic power in the future. The results provide a valuable reference for the rational and

effective utilization of renewable and sustainable solar energy. Although the prediction models have been crosschecked with previous studies, due to the lack of access to ground-measured photovoltaic power data, the forecasted photovoltaic power data are not very well validated with reliable measurements and may produce some bias in the PV power output values. A validated forecasting model with a photovoltaic power dataset will be presented in future works.

Acknowledgements

This work was financially supported by the National Natural Science Foundation of China (Grant No. 41801021 and Grant No. 41601044) and the International Postdoctoral Exchange Fellowship Program 2018 (Grant No. 20181010). We would like to thank the international modeling groups for providing their data

for analysis, the Program of Climate Model Diagnosis and Intercomparison (PCMDI), the World Climate Research Programme's (WCRP) Working Group on Coupled Modelling (WGCM) and the Coupled Model Intercomparison Project (CMIP) and the Institute for Climate and Atmospheric Sciences at ETH Zurich for providing the Global Energy Balance Archive (GEBA) database.

Appendix A. Supplementary data

Supplementary data related to this article can be found at <https://doi.org/10.1016/j.jclepro.2019.03.268>.

Appendix

Table A1
Information of 568 stations in GEBA.

No.	Station	Lat	Lon	Time series	No.	Station	Lat	Lon	Time series	No.	Station	Lat	Lon	Time series
1	57	24	32.8	1980–2000	191	1196	54.2	11.2	1964–1997	381	1684	46.6	7.12	1981–2010
2	61	30.2	31.3	1968–1999	192	1197	52.4	13.1	1937–2006	382	1690	58.5	26.8	1955–1994
3	69	6.55	5.62	1964–1992	193	1198	51.1	13.2	1964–1996	383	2039	45.8	127	1961–2010
4	72	11.9	-16	1958–1974	194	1199	50.4	12.2	1964–1998	384	2040	43.8	87.6	1959–2010
5	76	-0.2	20.9	1968–1981	195	1200	55	8.13	1973–1998	385	2041	41.7	123	1961–2010
6	83	-20	28.6	1955–1992	196	1201	54.5	9.55	1981–1998	386	2042	39.9	116	1957–2010
7	87	33.6	-7.7	1970–1994	197	1202	53.7	7.12	1966–1998	387	2043	36.1	104	1959–2003
8	99	-7.4	20.8	1958–1973	198	1203	53.7	10.2	1949–2010	388	2044	31.4	121	1991–2010
9	101	13.6	25.3	1958–1978	199	1204	53.1	8.13	1976–1998	389	2045	30.7	104	1961–2003
10	102	25.5	30.5	1972–1999	200	1205	52.3	10.2	1958–2010	390	2046	30.6	114	1961–2010
11	104	0.53	35.3	1974–1992	201	1206	52.3	8.05	1977–1998	391	2047	25	103	1961–2010
12	107	32.6	-17	1957–1972	202	1207	51.8	6.1	1973–1998	392	2048	23.1	113	1961–2010
13	109	-0.5	39.6	1966–1992	203	1208	51.8	8.13	1982–1998	393	2072	-22	114	1987–2006
14	130	-5.9	22.4	1958–1977	204	1209	51.7	10.2	1957–1998	394	2073	5.93	116	1989–2007
15	134	-27	18.1	1957–1976	205	1210	51.5	7.12	1973–1991	395	2077	42.6	9.15	1991–2010
16	138	-4.4	15.3	1954–1989	206	1211	51.3	9.15	1979–1998	396	2099	60.4	15.3	1989–2010
17	141	1.02	35	1966–1992	207	1212	50.7	7.12	1976–1998	397	2100	57.7	12.2	1988–2008
18	148	-8.8	13.2	1957–1973	208	1213	50.6	8.13	1981–1998	398	2101	59.4	13.2	1983–2010
19	152	9.55	31.7	1964–1983	209	1214	50.3	10.2	1981–1998	399	2102	55.7	13.2	1989–2010
20	154	-3.2	40.1	1968–1987	210	1215	50	7.12	1976–1998	400	2103	58.6	16.3	1989–2010
21	155	3.95	41.9	1967–1992	211	1216	49.8	9.97	1957–2007	401	2104	63.2	14.5	1983–2007
22	157	-26	32.6	1955–2005	212	1217	49.8	6.67	1958–2007	402	2105	63.8	20.3	1989–2010
23	165	16.9	-25	1957–1973	213	1218	49.5	8.13	1979–1998	403	2106	56.9	14.7	1983–2010
24	166	-15	12.2	1958–1973	214	1219	49.5	11.1	1976–1998	404	2107	57.7	18.4	1983–2010
25	168	-4	39.6	1964–1981	215	1220	49.2	7.12	1981–1998	405	2108	47.3	9.35	1981–2010
26	174	-1.3	36.8	1957–1992	216	1221	49	11	1981–1998	406	2110	46.8	6.95	1981–2010
27	180	-1.1	35.8	1979–1991	217	1222	48.8	9.2	1979–1998	407	2111	46.8	9.15	1988–2010
28	194	19.6	37.2	1958–1985	218	1223	48.6	13.5	1979–1996	408	2112	46.4	6.1	1981–2010
29	204	0.38	6.72	1959–1974	219	1224	48.4	11.7	1961–2010	409	2114	47.6	7.12	1989–2010
30	208	15.7	32.5	1964–1991	220	1225	48	7.12	1973–1998	410	2118	46.4	9.15	1981–2010
31	210	36.9	10.4	1964–2000	221	1226	47.8	11.2	1953–2005	411	2134	47.1	2.03	1987–2010
32	216	30.7	30.7	1972–1986	222	1227	55.7	12.3	1965–2001	412	2374	48.5	-105	1995–2010
33	221	-19	47.5	1954–1969	223	1228	43.5	-3.8	1986–2010	413	2377	34.3	-90	1995–2010
34	230	-3.4	38.6	1973–2003	224	1229	43.4	-5.9	1981–2010	414	2394	40.1	-89	1995–2010
35	231	14.4	33.5	1957–1991	225	1231	40.5	-3.1	1991–2010	415	2401	24.5	54.4	1982–1997
36	233	-23	17.1	1952–1976	226	1234	39.5	-6.1	1985–2000	416	2411	47.5	9.15	1994–2010
37	305	5.6	-0.2	1954–1979	227	1235	38	-1	1981–2010	417	2431	62.4	25.4	1991–2010
38	310	-29	26.3	1953–1976	228	1237	67.4	26.7	1953–2009	418	2450	43.4	-8.1	1995–2010
39	312	-34	18.6	1952–1976	229	1238	60.8	23.4	1957–2010	419	2471	43.5	5.08	1980–2010
40	313	-30	31	1952–1976	230	1239	60.2	24.4	1957–1991	420	2472	44.6	4.07	1994–2010
41	316	6.72	-1.6	1964–1984	231	1240	49.8	3.2	1973–1995	421	2488	56.5	-3.1	1988–2010
42	319	-25	31	1958–1975	232	1241	49.3	4.03	1974–2010	422	2490	50.9	5.08	1978–2010
43	320	-26	28.2	1952–1973	233	1242	49.2	0	1974–2010	423	2492	56.8	60.6	1964–1995
44	321	-26	28.4	1957–1976	234	1243	48.8	2.33	1978–1995	424	2493	53.3	50.5	1964–1993
45	324	4.88	-1.8	1965–1982	235	1245	48.8	2.02	1971–1995	425	2511	45	7.73	1964–1985
46	329	-24	29.5	1953–1968	236	1246	48.7	6.1	1967–2010	426	2515	45.8	21.3	1994–2010
47	421	49.2	-124	1964–1986	237	1247	48.6	7.63	1974–2010	427	2581	50.4	80.3	1965–1991
48	425	45.4	-76	1950–1982	238	1248	48.1	-1.7	1967–2010	428	2643	45.4	142	1961–2008
49	426	50.7	-127	1968–1977	239	1249	47.8	3.05	1977–2002	429	2646	43.8	142	1961–2008
50	436	50.3	-111	1961–1979	240	1250	47.5	0.72	1978–2010	430	2647	44.9	143	1975–2002
51	437	49.6	-120	1961–1985	241	1251	47.3	5.08	1977–2010	431	2648	44	142	1973–2002

(continued on next page)

Table A1 (continued)

No.	Station	Lat	Lon	Time series	No.	Station	Lat	Lon	Time series	No.	Station	Lat	Lon	Time series
52	438	50.3	-108	1961–1987	242	1252	47.2	-1	1986–2010	432	2649	42.9	143	1961–2008
53	440	43.7	-79	1960–1989	243	1255	46.3	4.07	1969–1995	433	2650	42.8	140	1973–2002
54	443	49.9	-97	1950–1984	244	1256	46.2	-1	1972–1995	434	2651	42.3	141	1973–2002
55	458	46.9	-68	1954–1966	245	1257	45.8	1.02	1968–2010	435	2652	42	143	1973–2002
56	459	32.9	-80	1951–1976	246	1258	45.8	3.05	1978–2010	436	2654	40.8	141	1961–2008
57	461	38.8	-92	1951–1976	247	1259	44.8	0	1978–2010	437	2655	40.5	142	1973–2002
58	463	31.8	-106	1952–1976	248	1260	44.6	6.1	1980–2010	438	2656	39.7	141	1961–2008
59	466	32.8	-97	1950–1971	249	1263	44.2	-1	1969–1996	439	2657	38.9	140	1961–2002
60	467	36.8	-120	1953–1976	250	1264	44.1	3.05	1967–2002	440	2658	38.3	140	1961–2007
61	468	48.2	-107	1959–1973	251	1265	44.1	5.05	1968–2000	441	2660	38.3	140	1961–2008
62	470	47.5	-111	1955–1974	252	1266	43.7	7.12	1971–2010	442	2661	37	141	1961–2008
63	471	36.1	-80	1956–1974	253	1267	43.6	3.05	1975–2010	443	2662	37.9	139	1972–2002
64	472	35.3	-76	1952–1974	254	1269	43.4	-0.4	1978–1995	444	2663	36.7	137	1961–2002
65	473	39.7	-86	1952–1965	255	1270	43.2	2.03	1980–1995	445	2664	37.1	138	1961–2007
66	474	30.1	-93	1954–1976	256	1272	42.7	2.87	1980–2010	446	2665	36.6	140	1961–2002
67	477	36.1	-115	1950–1969	257	1274	41.9	8.13	1970–2010	447	2666	36.1	136	1973–2002
68	478	34.7	-92	1953–1974	258	1276	60.1	-1	1952–2010	448	2667	36.4	139	1971–2002
69	479	33.9	-118	1953–1975	259	1278	57.2	-3.1	1984–2010	449	2668	35	137	1961–2008
70	481	42.4	-123	1953–1973	260	1279	57.2	-2	1968–2010	450	2669	35.7	139	1973–2002
71	482	25.8	-80	1952–1961	261	1283	55.3	-3.1	1956–2010	451	2670	35.7	141	1972–2002
72	485	36.1	-87	1965–1979	262	1284	54.7	-6.1	1968–2007	452	2671	34.6	138	1972–2002
73	487	36	-84	1950–1976	263	1285	53.8	-1	1959–1975	453	2673	35.7	140	1961–2008
74	488	35.4	-98	1952–1974	264	1286	53.8	-2	1959–1975	454	2675	35.5	135	1961–2008
75	490	33.4	-112	1952–1969	265	1289	52.8	-1.3	1959–1975	455	2676	34.9	132	1961–2002
76	492	44.1	-103	1952–1974	266	1290	52.7	1.02	1984–2000	456	2677	35.3	136	1961–2008
77	494	45.6	-94	1955–1974	267	1293	52.1	-4.1	1957–2010	457	2678	34	131	1961–2008
78	496	29.5	-98	1957–1972	268	1295	52	-0.4	1958–1975	458	2679	34.4	132	1961–2008
79	497	34.9	-120	1950–1974	269	1297	51.7	0	1957–1975	459	2680	34.7	136	1961–2008
80	498	46.5	-84	1954–1974	270	1299	51.5	0	1958–2006	460	2681	34.2	129	1961–2008
81	499	47.5	-122	1952–1976	271	1300	51.5	0	1951–1980	461	2682	33.3	130	1961–2008
82	503	28	-83	1953–1973	272	1301	51.4	0	1965–2000	462	2683	33.2	132	1961–2008
83	850	47.4	8.57	1981–2007	273	1303	50.2	-5.1	1984–2010	463	2684	32.7	130	1961–2008
84	863	22.3	114	1984–2007	274	1304	49.2	-2	1968–1999	464	2685	32.8	131	1961–2008
85	867	23.1	72.6	1964–2005	275	1311	38	23.4	1960–1985	465	2686	31.9	131	1961–2008
86	870	21.8	72.2	1968–1990	276	1317	47.7	16.6	1964–1989	466	2687	33.9	133	1961–2002
87	878	8.48	77	1989–2008	277	1319	47.5	21.4	1964–1985	467	2688	34.3	134	1961–2008
88	879	43.3	146	1961–2007	278	1320	47.4	19.3	1964–2006	468	2689	33.6	134	1961–2008
89	880	43.1	141	1958–2007	279	1322	46.9	19.3	1964–1980	469	2690	28.4	130	1961–2008
90	881	39.7	140	1961–2008	280	1324	46.9	20.5	1980–2006	470	2691	24.8	125	1961–2008
91	882	39.7	142	1961–2007	281	1329	55.4	-7.1	1982–2010	471	2692	25.8	131	1961–2008
92	883	38.3	140	1961–2007	282	1330	54.2	-10	1982–2010	472	2693	44	144	1961–2008
93	884	37.4	137	1972–2007	283	1331	54.2	-7.1	1982–2010	473	2703	35	138	1973–2002
94	885	36.3	138	1973–2005	284	1332	53.4	-6.1	1976–2010	474	2705	34.8	139	1972–2002
95	886	36.1	140	1958–2007	285	1333	53.1	-7.1	1971–2010	475	2706	33.1	140	1971–2002
96	887	35.4	133	1961–2007	286	1334	52.7	-7.1	1969–2009	476	2733	39.5	76	1958–2000
97	888	34.8	136	1967–2007	287	1335	51.9	-10	1964–2010	477	2734	36.4	94.9	1957–2000
98	889	33.6	130	1960–2009	288	1338	64.1	-22	1957–2005	478	2736	29.7	91.1	1961–2000
99	890	33.5	136	1961–2007	289	1339	46.5	11.2	1964–1989	479	2737	34.7	114	1961–2000
100	891	32.7	133	1961–2008	290	1340	46	13.2	1964–1988	480	2739	23.4	117	1961–2000
101	892	31.6	131	1961–2009	291	1341	45.9	7.7	1964–1980	481	2740	22.8	108	1961–2000
102	893	27.1	142	1970–2009	292	1342	45.7	13.8	1969–2001	482	2741	20	110	1961–2000
103	894	26.2	128	1962–2007	293	1343	45.4	9.15	1964–1985	483	2742	26.1	119	1961–2000
104	895	24.3	124	1964–2010	294	1344	45.5	12.3	1964–1989	484	2743	30.2	120	1961–2000
105	896	24.3	154	1970–2010	295	1345	45.2	7.65	1964–1985	485	2744	32	119	1961–2000
106	897	41.7	130	1965–1992	296	1347	44.5	11.2	1964–1989	486	2745	31.9	117	1961–2000
107	898	39	126	1965–1992	297	1348	44.4	8.13	1964–1989	487	2748	26.6	107	1961–2000
108	899	38	126	1965–1992	298	1352	44	8.13	1964–2003	488	2749	25.3	110	1961–2000
109	901	37.8	129	1986–2009	299	1353	43.7	10.4	1964–2003	489	2750	22	101	1961–2000
110	902	37.6	127	1986–2009	300	1358	42.4	14.2	1964–1987	490	2751	34.3	109	1961–2000
111	903	35.1	129	1986–2009	301	1359	42.1	12.2	1964–2010	491	2752	36.7	117	1961–2000
112	904	34.8	126	1986–2009	302	1360	41.8	12.6	1964–2009	492	2753	43.7	112	1957–2000
113	906	49.9	92.1	1964–2009	303	1361	41.5	15.3	1964–2010	493	2754	38.5	106	1961–2000
114	907	49.6	100	1964–2002	304	1364	40.9	9.5	1964–1988	494	2755	37.8	113	1961–2000
115	908	47.9	107	1964–2006	305	1365	40.9	14.2	1964–1989	495	2756	43.9	125	1959–2000
116	909	47.8	96.9	1964–1996	306	1367	40.7	17.3	1964–2005	496	2757	39.1	117	1959–2000
117	910	43.6	104	1966–1998	307	1368	40.6	8.13	1964–1989	497	2758	37.1	79.9	1957–2000
118	912	22.2	114	1964–1988	308	1369	40	15.3	1964–2003	498	2759	42.8	93.5	1961–2000
119	925	73.5	80.4	1938–1988	309	1370	39.3	9.15	1964–1995	499	2760	36.6	102	1959–2000
120	926	71	-179	1964–1994	310	1371	39	17.3	1964–1989	500	2761	50.3	127	1961–2000
121	927	70.6	162	1954–1993	311	1372	38.7	13.2	1964–1997	501	2769	47.7	88.1	1960–2000
122	929	67.6	133	1964–2003	312	1373	38.2	15.3	1964–2001	502	2770	44	81.3	1960–2000
123	930	65.8	88	1964–1995	313	1374	37.9	12.5	1964–1996	503	2771	40.2	94.7	1957–2000
124	931	63.3	143	1964–1987	314	1375	37.1	14.2	1966–1997	504	2772	32.5	80.1	1971–2000
125	932	62.1	130	1964–1987	315	1376	36.8	12	1964–1999	505	2773	31.2		

Table A1 (continued)

No.	Station	Lat	Lon	Time series	No.	Station	Lat	Lon	Time series	No.	Station	Lat	Lon	Time series
127	934	60.3	102	1964–1987	317	1380	52.9	4.07	1978–2010	507	2776	49.2	120	1960–2000
128	935	59.4	143	1964–1982	318	1381	52.1	5.08	1964–2009	508	2778	46.8	130	1961–2000
129	936	56.8	60.6	1964–1989	319	1382	51.5	3.6	1978–2009	509	2779	30.7	111	1961–2000
130	937	54.9	73.4	1964–2008	320	1384	60.4	5.08	1965–2010	510	2780	28.8	105	1984–2000
131	938	53.3	50.5	1964–1989	321	1386	54.2	15.3	1964–2010	511	2781	25	98.5	1961–2000
132	939	53	159	1964–1986	322	1389	52.3	21	1964–2010	512	2782	31.5	105	1978–2000
133	940	52.3	104	1964–1993	323	1391	51.8	20.3	1970–2010	513	2783	29.5	103	1961–2000
134	941	52	113	1964–1991	324	1393	49.3	20	1964–2010	514	2784	31.5	92.1	1961–2000
135	942	50.4	80.3	1964–1988	325	1395	41.8	-6.1	1964–2010	515	2785	33	97	1960–2000
136	943	48.5	135	1964–1986	326	1396	41.1	-8.6	1964–1989	516	2786	35.7	111	1961–2000
137	944	46.9	143	1964–1994	327	1397	40.4	-7.6	1964–1979	517	2787	40.1	113	1961–2000
138	946	46.8	61.7	1964–1979	328	1398	40.2	-8.1	1964–1989	518	2788	36	106	1985–2000
139	947	43.1	132	1964–1993	329	1400	38.7	-9.2	1964–2010	519	2789	39	88.2	1957–2000
140	948	41.3	69.3	1964–1992	330	1402	38.6	-7.1	1964–1989	520	2790	38.6	103	1961–2000
141	1044	43.8	-80	1969–1985	331	1403	37	-7.1	1964–1986	521	2791	25.9	115	1961–2000
142	1049	16.3	-62	1989–2009	332	1404	47.2	27.5	1964–2010	522	2792	42.9	89.2	1960–2000
143	1051	14.6	-61	1987–2007	333	1405	46.8	23.4	1964–2010	523	2802	36.1	114	1961–1990
144	1054	19.3	-99	1967–2006	334	1406	45.8	21.3	1964–1980	524	2804	43.6	122	1976–2000
145	1055	46.8	-56	1973–2009	335	1407	45.5	28.5	1970–2010	525	2805	42.8	129	1960–2000
146	1068	-12	131	1953–2001	336	1408	44.5	26.4	1964–2010	526	2806	41.6	120	1963–2000
147	1070	-16	150	1978–1993	337	1409	44.2	23.4	1988–2007	527	2807	38.9	122	1971–2000
148	1073	-18	128	1969–1986	338	1410	44.2	28.5	1970–2006	528	2812	26.9	100	1961–2000
149	1077	-20	119	1969–1991	339	1412	67.9	20.3	1970–2010	529	2813	23.4	103	1961–2000
150	1082	-24	134	1953–2000	340	1413	65.6	22.4	1965–2010	530	2823	32.2	116	1961–2000
151	1102	-33	152	1965–1982	341	1414	59.4	18	1922–2010	531	2832	41.8	82.9	1957–1990
152	1106	-34	142	1969–2004	342	1415	64.6	40.5	1964–1995	532	2834	40.7	111	1971–1991
153	1118	-38	141	1969–2005	343	1416	60	30.3	1964–1995	533	2835	39.4	110	1961–1991
154	1120	-38	145	1970–1992	344	1417	55.8	37.6	1964–2010	534	2836	37.5	121	1961–2000
155	1131	-18	177	1966–2008	345	1418	55.7	37.5	1971–1995	535	2837	29.5	104	1973–1990
156	1140	5.3	100	1975–2005	346	1419	54.9	23.4	1964–1993	536	2838	26.9	104	1961–1990
157	1141	3.12	102	1973–2007	347	1420	50.4	30.5	1964–2010	537	2840	30.3	121	1961–1990
158	1142	-21	164	1997–2010	348	1421	46.5	30.6	1964–2010	538	2841	28.2	113	1961–1987
159	1144	-37	175	1970–1989	349	1433	39.7	-32	1964–1981	539	2842	29.9	106	1961–1987
160	1145	-40	175	1965–1991	350	1434	38.7	-27	1964–1989	540	2843	31.2	121	1961–1990
161	1147	-41	175	1965–1991	351	1435	37.8	-26	1964–1985	541	2844	22.6	113	1965–1990
162	1148	-43	173	1965–1991	352	1436	46.1	14.2	1964–1991	542	2845	24.8	114	1961–1990
163	1149	-44	170	1967–1988	353	1438	45.9	16	1964–2004	543	2846	27.7	107	1961–1990
164	1150	-46	168	1965–1991	354	1439	45.8	16	1965–1987	544	2847	30.8	106	1973–1990
165	1153	14.6	121	1964–1996	355	1442	45.5	13.6	1974–1982	545	2848	30.8	108	1961–1990
166	1154	1.37	104	1965–2004	356	1444	44.8	20.3	1964–1991	546	2849	29.6	116	1961–1990
167	1156	19.3	167	1954–1976	357	1445	44.8	17.3	1964–1991	547	2851	32.7	109	1961–1990
168	1159	48.3	16.7	1967–1983	358	1449	43.5	16.4	1964–1979	548	2852	27.3	104	1961–1990
169	1162	48.1	14.6	1964–1984	359	1453	42.1	19.3	1965–1985	549	2854	35.5	117	1964–1990
170	1164	47.8	13.2	1965–1980	360	1456	41.1	21.4	1969–1988	550	2855	40.5	124	1961–1990
171	1165	47.8	13	1957–2003	361	1478	47.6	7.12	1981–2007	551	2867	52	5.65	1938–2006
172	1169	47.3	11.2	1969–1993	362	1479	48.3	16.4	1964–2010	552	3707	51.1	25.9	1994–2010
173	1171	47.1	13	1964–2010	363	1481	50.1	14.4	1986–2010	553	3750	46.9	8.15	1981–2007
174	1172	47	15.3	1964–2010	364	1569	46.8	9.15	1935–1977	554	3751	47	7.13	1981–2007
175	1173	46.7	14.2	1964–2010	365	1570	46.8	9.83	1947–2007	555	3752	45.9	7.12	1981–2007
176	1174	51.2	2.92	1968–1993	366	1572	47.5	8.53	1959–2010	556	3753	46.2	6.11	1981–2010
177	1175	51	3.05	1968–2007	367	1573	47.4	8.13	1969–1995	557	3754	46.6	8.15	1989–2007
178	1176	50.8	4.35	1961–2009	368	1593	47.7	9.15	1977–1993	558	3755	46.7	8.15	1981–2007
179	1179	50	5.4	1968–2007	369	1598	50.7	-1	1958–1975	559	3756	47.1	6.11	1981–2007
180	1181	43.2	27.9	1964–1991	370	1614	38.5	-122	1950–1969	560	3757	46	8.14	1981–2007
181	1182	42.7	23.3	1964–2009	371	1615	42.8	-84	1950–1969	561	3758	47	8.13	1981–2007
182	1183	42.6	23.4	1970–1989	372	1619	41.5	-71	1950–1969	562	3759	47.4	8.52	1981–2007
183	1187	46.8	9.15	1978–2007	373	1623	33.2	-84	1950–1966	563	3760	46.5	9.18	1982–2007
184	1188	46.2	8.13	1939–2010	374	1626	42.4	-77	1950–1969	564	3761	46.2	7.34	1981–2007
185	1189	50.3	15.3	1953–2010	375	1633	34.1	-118	1951–1969	565	3762	47.4	9.4	1981–2007
186	1190	49.8	18.2	1986–2010	376	1643	34	-117	1950–1969	566	3783	56.5	-3.1	1987–2007
187	1191	49.1	20.1	1973–1991	377	1653	40.8	-78	1950–1969	567	3811	-32	116	1975–1993
188	1192	49.1	13.2	1986–2010	378	1659	60.3	24.4	1971–2010	568	3816	21.5	40.6	1975–1990
189	1193	48.9	16.3	1986–2010	379	1661	62.4	25.4	1958–1980					
190	1195	48.2	17.3	1964–2010	380	1662	69.8	27	1972–2010					

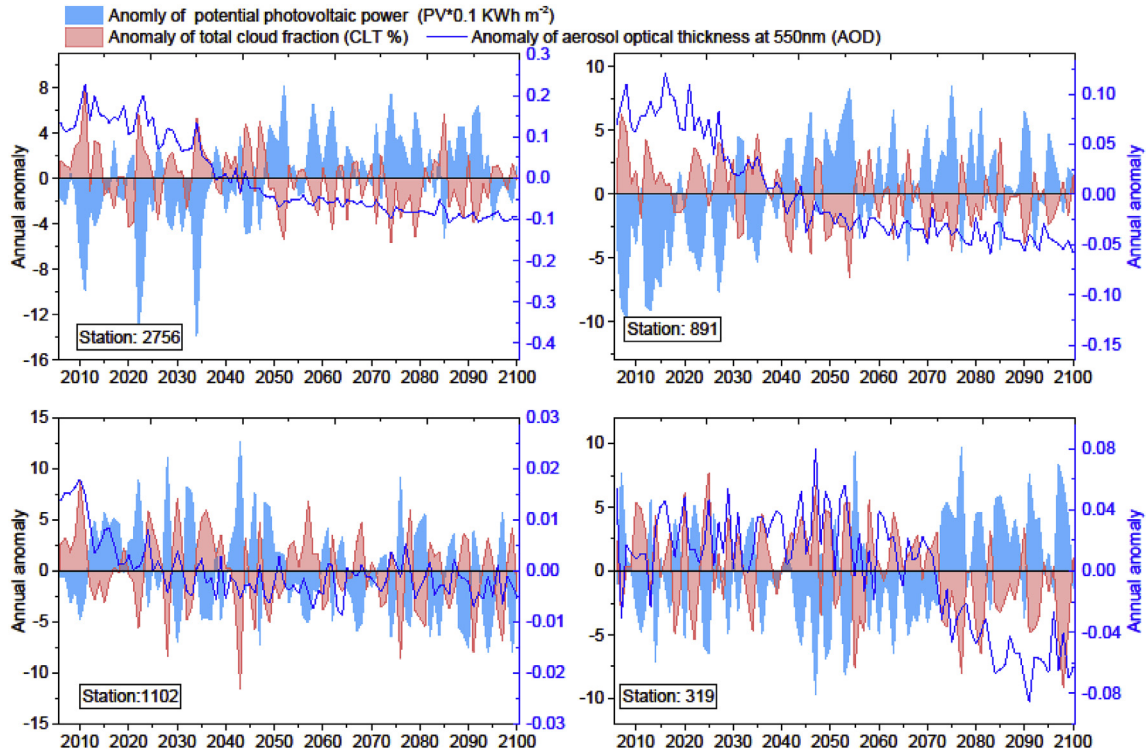


Fig. A1a. Anomaly variations of potential photovoltaic power (PV), aerosol optical thickness at 550 nm (AOD) and total cloud fraction (CLT) at stations 2756, 891, 1102 and 319.

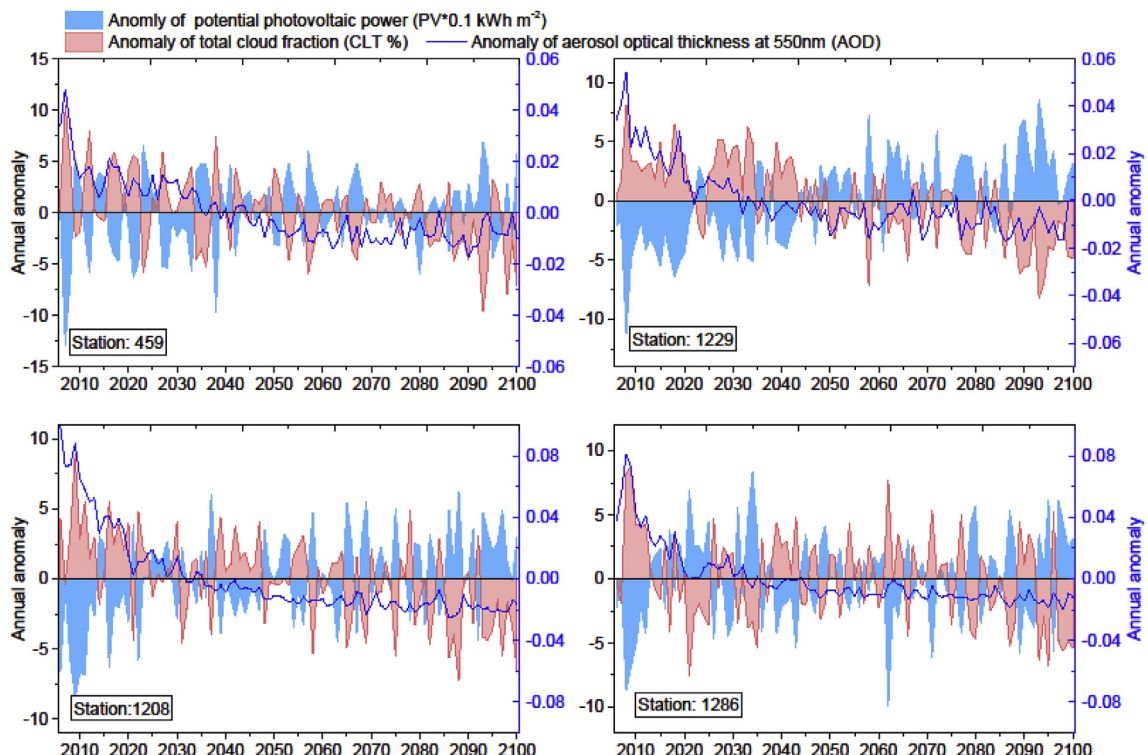


Fig. A1b. At stations 459, 1229, 1208 and 1286.

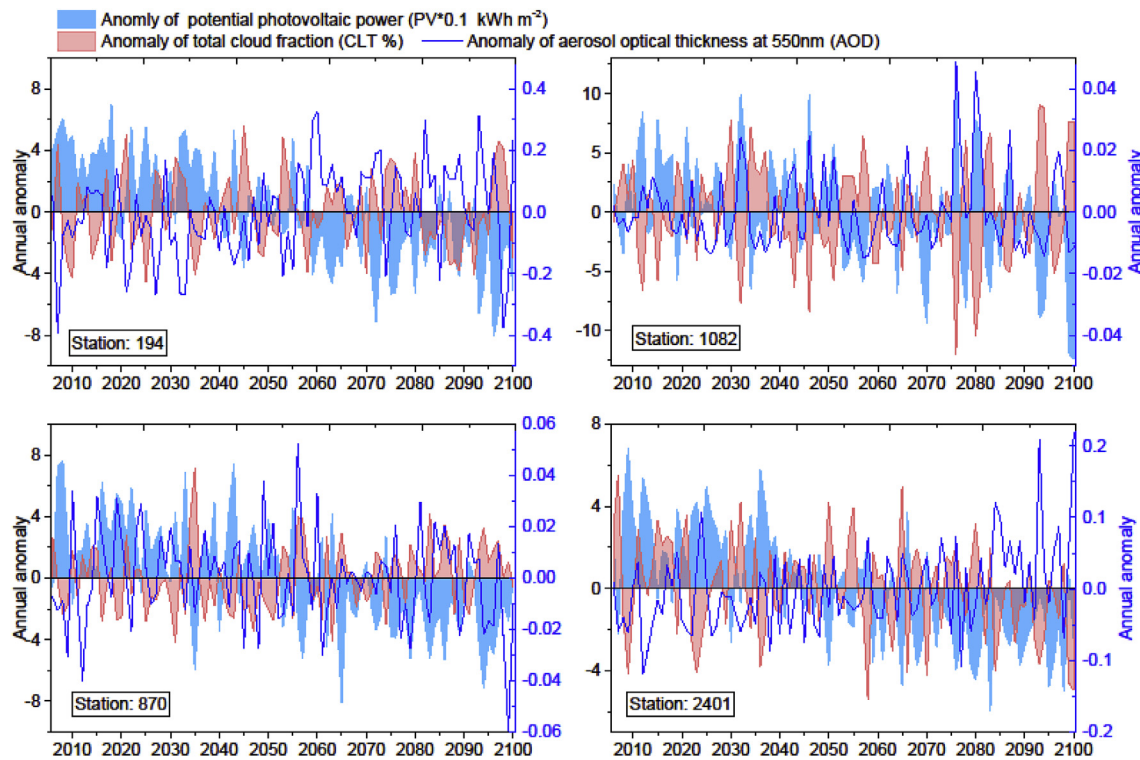


Fig. A1c. At stations 194, 1082, 870 and 2401.

References

- Alpert, P., Kishcha, P., Kaufman, Y.J., Schwarzbard, R., 2005. Global dimming or local dimming?: effect of urbanization on sunlight availability. *Geophys. Res. Lett.* 32, L17802. <https://doi.org/10.1029/2005GL023320>.
- Antonanzas, J., Osorio, N., Escobar, R., Urraca, R., Martinez-de-Pison, F.J., Antonanzas-Torres, F., 2016. Review of photovoltaic power forecasting. *Sol. Energy* 136, 78–111. <https://doi.org/10.1016/j.solener.2016.06.069>.
- Assoa, Y.B., Menezo, C., Fraisse, G., Yezou, R., Brau, J., 2007. Study of a new concept of photovoltaic–thermal hybrid collector. *Sol. Energy* 81 (9), 1132–1143. <https://doi.org/10.1016/j.solener.2007.04.001>.
- Bartók, B., Wild, M., Folini, D., Lüthi, D., Kotlarski, S., Schär, C., Vautard, R., Jerez, S., Imecs, Z., 2017. Projected changes in surface solar radiation in CMIP5 global climate models and in EURO-CORDEX regional climate models for Europe. *Clim. Dyn.* 49, 2665–2683. <https://doi.org/10.1007/s00382-016-3471-2>.
- Bayrakci, M., Choi, Y., Brownson, J.R.S., 2014. Temperature dependent power modeling of photovoltaics. *Energy Procedia* 57, 745–754. <https://doi.org/10.1016/j.egypro.2014.10.282>.
- Besharat, F., Dehghan, A.A., Faghih, A.R., 2013. Empirical models for estimating global solar radiation: a review and case study. *Renew. Sustain. Energy Rev.* 21, 798–821. <https://doi.org/10.1016/j.rser.2012.12.043>.
- Bizzarri, F., Bongiorno, M., Brambilla, A., Gruosso, G., Gajani, G.S., 2013. Model of photovoltaic power plants for performance analysis and production forecast. *IEEE Trans. Sustain. Energy* 4 (2), 278–285. <https://ieeexplore.ieee.org/document/6324407>.
- Bonanno, F., Capizzi, G., Graditi, G., Napoli, C., Tina, G.M., 2012. A radial basis function neural network based approach for the electrical characteristics estimation of a photovoltaic module. *Appl. Energy* 97, 956–961. <https://doi.org/10.1016/j.apenergy.2011.12.085>.
- BPSRWE, 2018. BP Statistical Review of World Energy, June 2018. London, United Kingdom. <https://www.bp.com/content/dam/bp/business-sites/en/global/corporate/pdfs/energy-economics/statistical-review/bp-stats-review-2018-full-report.pdf>.
- Cohen, S., Liepert, B., Stanhill, G., 2004. Global dimming comes of age. *Eos Trans. Am. Geophys. Union* 85 (38), 362. <https://agupubs.onlinelibrary.wiley.com/doi/pdf/10.1029/2004EO38004>.
- Crook, J.A., Jones, L.A., Forster, P.M., Crook, R., 2011. Climate change impacts on future photovoltaic and concentrated solar power energy output. *Energy Environ. Sci.* 4 (9), 3101–3109. <https://pubs.rsc.org/en/content/articlelanding/2011/ee/c1ee01495a#!divAbstract>.
- Ding, M., Wang, L., Bi, R., 2011. An ANN-based approach for forecasting the power output of photovoltaic system. *Procedia Environ. Sci.* 11 (1), 1308–1315. <https://doi.org/10.1016/j.proenv.2011.12.196>.
- Dubey, S., Sarvaiya, J.N., Seshadri, B., 2013. Temperature dependent photovoltaic (PV) efficiency and its effect on PV production in the world – a review. *Energy Procedia* 33, 311–321. <https://doi.org/10.1016/j.egypro.2013.05.072>.
- Duffie, J.A., Beckman, W.A., McGowan, J., 1980. *Solar Engineering of Thermal Processes*. A Wiley-Interscience.
- Evans, D.L., 1981. Simplified method for predicting photovoltaic array output. *Sol. Energy* 27 (6), 555–560. [https://doi.org/10.1016/0038-092X\(81\)90051-7](https://doi.org/10.1016/0038-092X(81)90051-7).
- Gaetani, M., Huld, T., Vignati, E., Monforti-Ferrario, F., Dosio, A., Raes, F., 2014. The near future availability of photovoltaic energy in Europe and Africa in climate-aerosol modeling experiments. *Renew. Sustain. Energy Rev.* 38, 706–716. <https://doi.org/10.1016/j.rser.2014.07.041>.
- Gilgen, H., Ohmura, A., 1999. The global energy balance archive. *Bull. Am. Meteorol. Soc.* 80 (5), 831–850. [https://doi.org/10.1175/1520-0477\(1999\)080<0831:TGEBA>2.0.CO;2](https://doi.org/10.1175/1520-0477(1999)080<0831:TGEBA>2.0.CO;2).
- Gilgen, H., Roesch, A., Wild, M., Ohmura, A., 2009. Decadal changes in shortwave irradiance at the surface in the period from 1960 to 2000 estimated from Global Energy Balance Archive Data. *J. Geophys. Res.: Atmospheres* 114, D00D08. <https://doi.org/10.1029/2008JD011383>.
- Gueymard, C., 1989. An atmospheric transmittance model for the calculation of the clear sky beam, diffuse and global photosynthetically active radiation. *Agric. For. Meteorol.* 45 (3), 215–229. [https://doi.org/10.1016/0168-1923\(89\)90045-2](https://doi.org/10.1016/0168-1923(89)90045-2).
- IEA, 2018. International Energy Agency – Tracking Clean Energy Progress. Paris, France. <https://www.iea.org/tcep/power/renewables/solar/>.
- Jahani, B., Dinipashoh, Y., Raisi Naqchi, A., 2017. Evaluation and development of empirical models for estimating daily solar radiation. *Renew. Sustain. Energy Rev.* 73, 878–891. <https://doi.org/10.1016/j.rser.2017.01.124>.
- Jerez, S., Thais, F., Tobin, I., Wild, M., Colette, A., Yiou, P., Vautard, R., 2015. The CLIMIX model: a tool to create and evaluate spatially-resolved scenarios of photovoltaic and wind power development. *Renew. Sustain. Energy Rev.* 42, 1–15. <https://doi.org/10.1016/j.rser.2014.09.041>.
- Kendall, M.G., 1948. *Rank Correlation Methods*. Charles Griffin and Company, London.
- Li, Z., Whitlock, C.H., Charlock, T.P., 1995. Assessment of the global monthly mean surface insolation estimated from satellite measurements using global energy balance archive data. *J. Clim.* 8 (2), 315–328. [https://doi.org/10.1175/1520-0442\(1995\)008<0315:AOTGMM>2.0.CO;2](https://doi.org/10.1175/1520-0442(1995)008<0315:AOTGMM>2.0.CO;2).
- Liepert, B., Tegen, I., 2002. Multidecadal solar radiation trends in the United States and Germany and direct tropospheric aerosol forcing. *J. Geophys. Res.: Atmospheres* 107 (D12), 4153. <https://doi.org/10.1029/2001JD000760>.
- Liepert, B.G., 2002. Observed reductions of surface solar radiation at sites in the United States and worldwide from 1961 to 1990. *Geophys. Res. Lett.* 29 (10), 61–64. <https://doi.org/10.1029/2002GL014910>.
- Loew, A., Andersson, A., Trentmann, J., Schröder, M., 2016. Assessing surface solar radiation fluxes in the CMIP ensembles. *J. Clim.* 29 (20), 7231–7246. <https://doi.org/10.1175/JCLI-D-14-00503.1>.
- Long, C.N., Dutton, E.G., Augustine, J.A., Wiscombe, W., Wild, M., McFarlane, S.A., Flynn, C.J., 2009. Significant decadal brightening of downwelling shortwave in the continental United States. *J. Geophys. Res.: Atmospheres* 114, D00D06. <https://doi.org/10.1029/2008JD011263>.

- Lorenz, E., Scheidsteger, T., Hurka, J., Heinemann, D., Kurz, C., 2011. Regional PV power prediction for improved grid integration. *Prog. Photovoltaics Res. Appl.* 19 (7), 757–771. <https://doi.org/10.1002/pip.1033>.
- Müller, R., Pfeifroth, U., Träger-Chatterjee, C., Trentmann, J., Cremer, R., 2015. Digging the METEOSAT treasure-3 decades of solar surface radiation. *Rem. Sens.* 7 (6), 8067. <https://doi.org/10.3390/rs70608067>.
- Ma, Q., Wang, K., Wild, M., 2015. Impact of geolocations of validation data on the evaluation of surface incident shortwave radiation from Earth System Models. *J. Geophys. Res.: Atmospheres* 120 (14), 6825–6844. <https://doi.org/10.1002/2014JD022572>.
- Mann, H.B., 1945. Nonparametric tests against trend. *Econometrica* 13, 245–259. <https://doi.org/10.2307/1907187>.
- Mellit, A., 2008. Artificial Intelligence technique for modelling and forecasting of solar radiation data: a review. *Int. J. Artif. Intell. Soft Comput.* 1 (1), 52–76. <https://doi.org/10.1504/IJAISC.2008.021264>.
- Nabat, P., Somot, S., Mallet, M., Chiapello, I., Morcrette, J.J., Solmon, F., Szopa, S., Dulac, F., Collins, W., Ghan, S., Horowitz, L.W., Lamarque, J.F., Lee, Y.H., Naik, V., Nagashima, T., Shindell, D., Skeie, R., 2013. A 4-D climatology (1979–2009) of the monthly tropospheric aerosol optical depth distribution over the Mediterranean region from a comparative evaluation and blending of remote sensing and model products. *Atmos. Meas. Tech.* 6 (5), 1287–1314. <https://doi.org/10.5194/amt-6-1287-2013>.
- Norris, J.R., Wild, M., 2009. Trends in aerosols radiative effects over China and Japan inferred from observed cloud cover, solar “dimming,” and solar “brightening”. *J. Geophys. Res.: Atmospheres* 114, D00D15. <https://doi.org/10.1029/2008JD011378>.
- Notton, G., Cristofari, C., Mattei, M., Poggi, P., 2005. Modelling of a double-glass photovoltaic module using finite differences. *Appl. Therm. Eng.* 25 (17), 2854–2877. <https://doi.org/10.1016/j.applthermaleng.2005.02.008>.
- Ohmura, A., 2009. Observed decadal variations in surface solar radiation and their causes. *J. Geophys. Res.: Atmospheres* 114, D00D05. <https://doi.org/10.1029/2008JD011290>.
- Padma Kumari, B., Londhe, A., Daniel, S., Jadhav, D., 2007. Observational evidence of solar dimming: offsetting surface warming over India. *Geophys. Res. Lett.* 34 (21), L21810. <https://doi.org/10.1029/2007GL031133>.
- Padmakumari, B., Soni, V.K., Rajeevan, M.N., 2017. Trends in radiative fluxes over the Indian region. In: Rajeevan, M.N., Nayak, S. (Eds.), *Observed Climate Variability and Change over the Indian Region*. Springer Singapore, Singapore, pp. 145–163. https://doi.org/10.1007/978-981-10-2531-0_9.
- Paulescu, M., Paulescu, E., Gravila, P., Badescu, V., 2013. Solar radiation measurements. In: Paulescu, M., Paulescu, E., Gravila, P., Badescu, V. (Eds.), *Weather Modeling and Forecasting of PV Systems Operation*. Springer London, London, pp. 17–42.
- Práválie, R., Patriche, C., Bandoc, G., 2019. Spatial assessment of solar energy potential at global scale. A geographical approach. *J. Clean. Prod.* 209, 692–721. <https://doi.org/10.1016/j.jclepro.2018.10.239>.
- Qazi, A., Fayaz, H., Wadi, A., Raj, R.G., Rahim, N., Khan, W.A., 2015. The artificial neural network for solar radiation prediction and designing solar systems: a systematic literature review. *J. Clean. Prod.* 104, 1–12. <https://doi.org/10.1016/j.jclepro.2015.04.041>.
- Rana, M., Koprinska, I., Agelidis, V.G., 2016. Univariate and multivariate methods for very short-term solar photovoltaic power forecasting. *Energy Convers. Manag.* 121, 380–390. <https://doi.org/10.1016/j.enconman.2016.05.025>.
- REN, 2017. Renewables 2017 - global status report. In: Renewable Energy Policy Network for the 21st Century. Paris, France. <http://www.ren21.net/gsr-2017>.
- REN, 2018. Renewables 2018 - global status report. In: Renewable Energy Policy Network for the 21st Century. Paris, France. <http://www.ren21.net/gsr-2018>.
- Ritchie, H., Roser, M., 2019. Renewable Energy. Published online at [OurWorldInData.org](https://ourworldindata.org/). <https://ourworldindata.org/renewable-energy>.
- Sanchez-Lorenzo, A., Wild, M., Brunetti, M., Guijarro, J.A., Hakuba, M., Calbó, J., Mystakidis, S., Bartok, B., 2015. Reassessment and update of long-term trends in downward surface shortwave radiation over Europe (1939–2012). *J. Geophys. Res.: Atmospheres* 120 (18), 9555–9569. <https://doi.org/10.1002/2015JD023321>.
- Schmelas, M., Feldmann, T., da Costa Fernandes, J., Bollin, E., 2015. Photovoltaics energy prediction under complex conditions for a predictive energy management system. *J. Sol. Energy Eng.* 137 (3), 031015. <https://doi.org/10.1115/1.4029378>.
- Sen, P.K., 1968. Estimates of the regression coefficient based on Kendall's tau. *J. Am. Stat. Assoc.* 63 (324), 1379–1389. <https://doi.org/10.1080/01621459.1968.10480934>.
- Skoplaki, E., Palyvos, J.A., 2009. On the temperature dependence of photovoltaic module electrical performance: a review of efficiency/power correlations. *Sol. Energy* 83 (5), 614–624. <https://doi.org/10.1016/j.solener.2008.10.008>.
- Stanhill, G., Cohen, S., 2001. Global dimming: a review of the evidence for a widespread and significant reduction in global radiation with discussion of its probable causes and possible agricultural consequences. *Agric. For. Meteorol.* 107 (4), 255–278. [https://doi.org/10.1016/S0168-1923\(00\)00241-0](https://doi.org/10.1016/S0168-1923(00)00241-0).
- Tang, W., Yang, K., Qin, J., Niu, X., Lin, C., Jing, X., 2017. A revisit to decadal change of aerosol optical depth and its impact on global radiation over China. *Atmos. Environ.* 150, 106–115. <https://doi.org/10.1016/j.atmosenv.2016.11.043>.
- Taylor, K.E., 2009. A Summary of the CMIP5 Experiment Design. LLNL report. http://cmip-pcmdi.llnl.gov/cmip5/docs/Taylor_CMIP5_design.pdf.
- Taylor, K.E., Stouffer, R.J., Meehl, G.A., 2012. An overview of CMIP5 and the experiment design. *Bull. Am. Meteorol. Soc.* 93 (4), 485–498. <https://doi.org/10.1175/BAMS-D-11-00094.1>.
- Voyant, C., Notton, G., Kalogirou, S., Nivet, M.-L., Paoli, C., Motte, F., Fouillot, A., 2017. Machine learning methods for solar radiation forecasting: a review. *Renew. Energy* 105, 569–582. <https://doi.org/10.1016/j.renene.2016.12.095>.
- Wang, Y., Wild, M., 2016. A new look at solar dimming and brightening in China. *Geophys. Res. Lett.* 43 (22). <https://doi.org/10.1002/2016GL071009>.
- Wild, M., 2009. Global dimming and brightening: a review. *J. Geophys. Res.: Atmospheres* 114, D00D16. <https://doi.org/10.1029/2008JD011470>.
- Wild, M., 2012. Enlightening global dimming and brightening. *Bull. Am. Meteorol. Soc.* 93 (1), 27–37. <https://doi.org/10.1175/BAMS-D-11-00074.1>.
- Wild, M., 2014. Global dimming and brightening. In: Freedman, B. (Ed.), *Global Environmental Change*. Springer Netherlands, Dordrecht, pp. 39–47. https://doi.org/10.1007/978-94-007-5784-4_27.
- Wild, M., Folini, D., Hakuba, M.Z., Schär, C., Seneviratne, S.I., Kato, S., Rutan, D., Ammann, C., Wood, E.F., König-Langlo, G., 2015a. The energy balance over land and oceans: an assessment based on direct observations and CMIP5 climate models. *Clim. Dyn.* 44 (11), 3393–3429. <https://doi.org/10.1007/s00382-014-2430-z>.
- Wild, M., Folini, D., Henschel, F., Fischer, N., Müller, B., 2015b. Projections of long-term changes in solar radiation based on CMIP5 climate models and their influence on energy yields of photovoltaic systems. *Sol. Energy* 116, 12–24. <https://doi.org/10.1016/j.solener.2015.03.039>.
- Wild, M., Gilgen, H., Roesch, A., Ohmura, A., Long, C.N., Dutton, E.G., Forgan, B., Kallis, A., Russak, V., Tsvetkov, A., 2005. From dimming to brightening: decadal changes in solar radiation at Earth's surface. *Science* 308 (5723), 847–850. <https://doi.org/10.1126/science.1103215>.
- Wild, M., Ohmura, A., Schär, C., Müller, G., Folini, D., Schwarz, M., Hakuba, M.Z., Sanchez-Lorenzo, A., 2017. The Global Energy Balance Archive (GEBA) version 2017: a database for worldwide measured surface energy fluxes. *Earth Syst. Sci. Data* 9 (2), 601–613. <https://doi.org/10.5194/essd-9-601-2017>.
- Wild, M., Trüssel, B., Ohmura, A., Long, C.N., König-Langlo, G., Dutton, E.G., Tsvetkov, A., 2009. Global dimming and brightening: an update beyond 2000. *J. Geophys. Res.: Atmospheres* 114, D00D13. <https://doi.org/10.1029/2008JD011382>.
- Xia, X., 2010. A closer looking at dimming and brightening in China during 1961–2005. *Ann. Geophys.* 28, 1121–1132. <https://doi.org/10.5194/angeo-28-1121-2010>.
- Yang, C., Xie, L., 2012. A Novel ARX-Based Multi-Scale Spatio-Temporal Solar Power Forecast Model, 2012. North American Power Symposium (NAPS), Champaign, IL, pp. 1–6. <https://doi.org/10.1109/NAPS.2012.6336383>.
- Yang, K., Koike, T., Ye, B., 2006. Improving estimation of hourly, daily, and monthly solar radiation by importing global data sets. *Agric. For. Meteorol.* 137 (1–2), 43–55. <https://doi.org/10.1016/j.agrformet.2006.02.001>.
- Yona, A., Senju, T., Funabashi, T., Kim, C.H., 2013. Determination method of insolation prediction with fuzzy and applying neural network for long-term ahead PV power output correction. *IEEE Trans. Sustain. Energy* 4 (2), 527–533. <https://doi.org/10.1109/TSTE.2013.2246591>.
- Zhang, X., Liang, S., Wang, G., Yao, Y., Jiang, B., Cheng, J., 2016. Evaluation of the reanalysis surface incident shortwave radiation products from NCEP, ECMWF, GSFC, and JMA using satellite and surface observations. *Rem. Sens.* 8 (3), 225. <https://doi.org/10.3390/rs8030225>.